Acidification, warming, and nutrient management are projected to cause reductions in shell and tissue weights of oysters in a coastal plain estuary

Catherine R. Czajka[1], Marjorie A.M. Friedrichs[1], Emily B. Rivest[1], Pierre St-Laurent[1], Mark J. Brush[1], and Fei Da[2]

[1]Virginia Institute of Marine Science, William & Mary, Gloucester Point, VA, 23062, USA
[2]Department of Geosciences, Princeton University, Princeton, NJ, 08544, USA

Correspondence to: Catherine R. Czajka (czajkacatherine@gmail.com)

Abstract. Coastal acidification, warming, and nutrient management actions all alter water quality conditions that marine species experience, with potential impacts to their physiological processes. Decreases in calcite saturation state (Ω_{Ca}) and food availability, combined with warming water temperatures, pose a threat to calcifying organisms; however, the magnitude of future changes in estuarine systems is challenging to predict and is not well known. This study aims to determine how and where oysters will be affected by future acidification, warming, and nutrient reductions, and the relative effects of these stressors. To address these goals, an oyster bioenergetics model for Eastern oysters (*Crassostrea virginica*) was embedded in a 3-D coupled hydrodynamic-biogeochemistry model implemented for two tributaries in the lower Chesapeake Bay. Model simulations were forced with projected future conditions (mid-21st century atmospheric CO_2 and atmospheric temperature under representative concentration pathway (RCP) 8.5, as well as managed nutrient reductions) and compared with a realistic present-day reference run. Together, all three stressors are projected to reduce Ω_{Ca} and growth of oyster shell and tissue. Increased atmospheric CO_2 and temperature are both projected to cause widespread reductions in Ω_{Ca}. The resulting reductions in oyster shell and tissue growth will be most severe along the tributary shoals. Future warming during peak oyster growing seasons is projected to have the strongest negative influence on tissue and shell growth, due to summer water temperatures reducing filtration rates, enhancing shell dissolution and oyster respiration rates, and increasing organic matter remineralization rates, thus reducing food availability. Nutrient reductions will exacerbate deficits in oyster food availability, contributing to further reductions in growth. Quantifying the effects of these stressors provides insight on the areas in the lower bay where oysters will be most vulnerable to mid 21st-century conditions.

Short summary. Under future acidification, warming, and nutrient management, substantial reductions in shell and tissue weights of Eastern oysters are projected for the Chesapeake Bay. Lower oyster growth rates will be largely driven by reduced calcium carbonate saturation states and reduced food availability. Oyster aquaculture practices in the region will likely be affected, with site selection becoming increasingly important as impacts will be highly spatially variable.

1 Introduction

Anthropogenic climate change and its associated impacts on water quality may threaten marine organisms and economic systems reliant on them. Oceanic uptake of increasing anthropogenic atmospheric carbon dioxide (CO_2) causes a decrease in seawater pH and saturation states of calcium carbonate (e.g., Ω_{Ca}), a phenomenon known as ocean acidification (Caldeira and Wickett, 2003; Doney et al., 2009). Globally, the ocean has absorbed about 30% of anthropogenic atmospheric CO_2 since pre-industrial times (Gruber et al., 2019), and open-ocean surface pH is anticipated to decrease by 0.3 units on average relative to the 2010s by the end of the century under 'business-as-usual' conditions (Riahi et al., 2011; IPCC, 2019). The percent volume of ocean water undersaturated with calcite ($\Omega_{Ca} < 1$), a condition associated with elevated energetic costs of shell-building for calcifying organisms, is predicted to expand to 91% by 2100 from 76% in the 1990s (Caldeira and Wicket, 2005; Gattuso et al., 2015). Concurrently, the global ocean has absorbed approximately 93% of the atmospheric heat produced by anthropogenic activity, leading to a global sea surface temperature increase of 0.7°C since 1900 (Jewett and Romanou, 2017). Ocean warming is expected to continue, with global averages increasing by 2.7°C by 2100 and greater increases expected in shallow coastal regions (Jewett and Romanou, 2017).

Since estuaries have lower and more variable pH than the open-ocean, the effects of increased CO_2 and warming on estuarine water quality and biota are often amplified. In coastal and estuarine systems, acidification may be exacerbated by local-level processes, such as the input of acidic freshwater and nutrient runoff from precipitation, a process termed coastal acidification (Salisbury et al., 2008; Wallace et al., 2014; Carstensen and Duarte, 2019). Coastal acidification may accelerate as warming of coastal waters increases rates of biogeochemical processes; increased respiration rates may drive larger diel variations in pH, dissolved oxygen, and associated water quality (Du et al., 2018; Tian et al., 2021). Freshwater has relatively low total alkalinity (TA), or buffering capacity, so estuarine areas with greater relative freshwater influence cannot resist changes to pH as easily as more saline or open-ocean waters (Hasler et al., 2018; Pacella et al., 2024). Eutrophication, the increased rate of organic matter input to a system (Nixon, 1995), may also drive large variations in local pH and overall water quality. Elevated nutrient inputs cause pH to increase in surface waters due to higher primary productivity, which will reduce surface acidification; however, pH will decrease in deeper bottom waters as the additional organic matter sinks and is remineralized (Cai et al., 2021). Management actions to reduce eutrophication and improve water quality in bottom waters have been successful but may also enhance acidification in shallow surface waters by lowering primary productivity (Borges and Gypens, 2010; Da et al., 2021). The overall effect of future changes in nutrient inputs on coastal biogeochemistry is thus unclear, particularly in the presence of warming and acidification.

Characterizing spatiotemporal patterns of acidification in estuarine waters is important, as negative impacts of acidification on the biology of marine organisms may be substantial. Acidification disrupts the formation of calcium carbonate ($CaCO_3$) during shell-building, i.e., biocalcification, which is a vital process for growth and survival of many aquatic invertebrate species (e.g., Orr et al., 2005; Gazeau et al., 2007; Dong et al., 2023). Under acidified conditions, water concentrations of CO_2 and H^+ increase, and concentrations of carbonate ions ($[CO_3^{2-}]$) decrease. A low ambient $[CO_3^{2-}]$ inhibits

64 calcifying organisms from forming $CaCO_3$ for their shells, as more energy is required to precipitate CO_3^{2-} from acidified waters

65 (e.g., Guinotte and Fabry, 2008; Lutier et al., 2022; Matoo et al., 2020; Mederios and Souza, 2023). Low Ω_{Ca} may also lead to

66 net dissolution of $CaCO_3$, leading to weaker shells and greater juvenile susceptibility to predation (e.g., Waldbusser et al.,

67 2011; Amaral et al., 2012; Barclay et al., 2020). Acidification may further reduce shell growth through adverse physiological

68 effects that limit energy availability for calcification. Because acidification is often more extreme in estuaries, coastal bivalve

69 species experience stronger effects of climate change than organisms living in open-ocean environments (Poach et al., 2019;

70 Melzner et al., 2020; Cai et al., 2021). Oysters in particular are of high management and research interest due to their

71 commercial value in the United States (USDA, 2023). Prior experiments have revealed negative effects of acidification,

72 warming, and nutrient reductions on oyster biocalcification and growth (Beniash et al., 2010; Waldbusser et al., 2011; Gobler

73 and Talmage, 2014), but it is yet to be determined how the impacts of these stressors on oyster shell and tissue growth will

74 vary spatially in highly dynamic systems.

75   The Chesapeake Bay is an excellent study system for examining the interacting influences of acidification, warming,

76 and nutrient reductions (hereafter referred to collectively as "future stressors") on estuarine biogeochemistry and the organisms

77 living there. The bay exhibits high temporal and spatial variability in pH due to seasonal phytoplankton blooms, eutrophication,

78 and acidic freshwater input (Da et al., 2021; St-Laurent et al., 2020; Kemp et al., 2005; Cai et al., 2021). From the mid-1980s

79 to mid-2010s, surface waters in the upper bay experienced pH increases between +0.2 and +0.4 pH units in early spring and

80 fall due to increased riverine TA from reduced acid mine drainage and lowered nitrate inputs, while surface waters in the

81 nitrogen-limited middle bay decreased up to -0.24 pH units during late spring and summer as a result of decreased primary

82 production (Da et al., 2021). Over the same time period, the bay warmed by $0.24 \pm 0.15°C$ per decade (Hinson et al., 2022),

83 more than double the average rate of warming for the upper 75m of the global ocean (Rhein et al., 2013). Warming has also

84 led to more severe hypoxia (Irby et al., 2018; Ni et al., 2020; Frankel et al., 2022; Hinson et al., 2023; Hinson et al., 2024). In

85 2010, the Environmental Protection Agency mandated a Total Maximum Daily Load (TMDL) of pollutants from point and

86 non-point sources to be achieved by 2025 (EPA, 2010). As nutrient reductions negatively affect pH in surface waters of the

87 bay (Shen et al., 2020; Da et al., 2021), achieving the TMDLs may actually worsen acidification in shallow and near-shore

88 regions. Much of the research effort devoted to characterizing present-day carbonate chemistry and its historical trends has

89 focused on the mainstem and upper Chesapeake Bay (Cai et al., 2017; Shen et al., 2020, Su et al., 2020), and less is known

90 about these conditions throughout the tributaries of the lower bay (Shadwick et al., 2019).

91   The combined effects of future stressors will impact calcifying organisms in the lower Chesapeake Bay as well as the

92 economic systems reliant upon them. The Eastern oyster *Crassostrea virginica* (Gmelin, 1791) is a foundation species native

93 to the bay (Dayton, 1972). Eastern oyster aquaculture in this region has grown rapidly in the past few decades, with Virginia

94 becoming the third most productive oyster fishery in 2018 (Hudson, 2019), largely a result of the development of disease-

95 resistant oyster strains (Frank-Lawale et al., 2014). Negative impacts of acidification on aquaculture practices in other parts of

96 the world (Barton et al., 2015) have already stirred concern over the vulnerability of oysters in the Chesapeake Bay. For

97 example, in the Pacific Northwest, major larval mortality occurred at a shellfish hatchery following an upwelling event that

98   lowered pH and Ω of aragonite, which had cascading impacts on the oyster industry all along the West Coast (Barton et al.,

99   2015). While most effects of acidification on aquaculture have been observed in oyster larvae in hatcheries, fewer studies have

100   examined acidification's influence on adult oysters when deployed in the field. Water quality conditions within oyster farms

101   can be highly spatially variable, so the impacts of acidification may vary with growing conditions (Saavedra et al., 2024;

102   Simpson et al., 2024). To support the future of the oyster aquaculture industry in Chesapeake Bay, it is critical to identify

103   which areas in the bay will be most vulnerable to acidification at mid-century and how each driver of change contributes to

104   acidification and its impacts on growth.

105   This study addresses the following primary research question: How and where will carbonate chemistry and Eastern

106   oyster growth in the lower Chesapeake Bay change in the future and which future stressors will drive these changes? A three-

107   dimensional hydrodynamic-biogeochemical model is coupled with an oyster bioenergetics model and is applied to two major

108   Virginia tributaries of the Chesapeake Bay. The model provides detailed information on present-day environmental conditions,

109   and when combined with climate projections from Earth System Models, allows for simulations of the independent and

110   interacting influences of future environmental change on carbonate chemistry and Eastern oysters. This study provides insight

111   into which areas are most vulnerable to mid 21st-century acidification and how acidification, warming, and nutrient loading

112   may each impact oyster growth in isolation as well as via simultaneous co-stressors.

113   **2 Methods**

114   **2.1 Model description**

115   **2.1.1 Hydrodynamic model**

116   This study uses the three-dimensional hydrodynamic Regional Ocean Modeling System (ROMS; Shchepetkin and

117   McWilliams, 2005), implemented similarly to St-Laurent and Friedrichs (2024) but on a higher resolution grid focused on two

118   of the lower Virginia Chesapeake Bay tributaries (Fig. 1). The model domain (Da et al., 2024) includes the York and

119   Rappahannock Rivers, as well as a portion of the mainstem shoal north of the Rappahannock. The model grid consists of

120   620x740 horizontal grid cells with a horizontal resolution of 120 m, allowing for greater resolution of coastlines than many

121   other Chesapeake Bay model grids (Irby et al., 2016). The hydrodynamic model includes 20 terrain-following vertical levels

122   and two primary state variables: practical salinity and potential temperature. A wetting and drying scheme has been

123   implemented to represent water levels and currents in coastal grid cells (Warner et al., 2013; St-Laurent and Friedrichs, 2024).

124   **2.1.2 Carbon and biogeochemistry model**

125   The Estuarine-Carbon-Biogeochemistry model (ECB) embedded in ROMS and used in this study has previously been

126   implemented in the Chesapeake Bay (Feng et al., 2015; St-Laurent et al., 2020; Frankel et al., 2022; Hinson et al., 2023) as

127   well as in the lower Virginia tributaries (Da et al., 2024). ECB simulates full carbon and nitrogen cycles of the lower trophic

128 levels, represented by the following state variables: nitrate, ammonium, phytoplankton and zooplankton nitrogen, small and

129 large detrital nitrogen and carbon, semi-labile and refractory dissolved organic nitrogen, DIC, TA, and dissolved oxygen (O_2).

130 Phytoplankton and zooplankton carbon are calculated from fixed C:N ratios (Redfield, 1934; Hopkinson et al., 1998). C:N

131 ratios for dissolved organic matter in the estuary are allowed to freely evolve with time. Biogeochemical processes include

132 primary production, aggregation, sinking, basal metabolism, exudation, sloppy feeding, excretion, metabolism,

133 nitrification/denitrification, remineralization, grazing, and mortality. Biogeochemical sources and sinks are included in the

134 bottom vertical level (e.g., burial, resuspension, nitrification/denitrification, remineralization, sediment O_2 and CO_2 exchange).

135 Light attenuation throughout the water column is based on the diffuse attenuation coefficient (Kd), which is parameterized as

136 a function of surface total suspended solids (TSS; including inorganic and organic components) and salinity as a proxy for

137 colored dissolved organic matter (Feng et al., 2015; Turner et al., 2021). TSS is calculated within the model as the sum of the

138 four inorganic suspended sediment size classes and particulate organic matter. Particulate organic carbon (POC) is calculated

139 as the sum of phytoplankton carbon, zooplankton carbon, and small and large detrital carbon. The sediment transport module

140 within ECB accounts for sediment-water exchange processes, such as deposition and resuspension of inorganic sediment and

141 particulate organic matter, and is comprised of two vertical seabed layers that simulate four suspended sediment size classes

142 (Turner et al., 2021).

143   The inorganic carbon module within ECB has been fine-tuned in this implementation of the model, allowing for

144 improved performance in carbonate system simulations (Da et al., 2024). The model grid includes tidal wetlands along the

145 York River based on estimated wetland areas (Mitchell et al., 2017), which further contribute to TA fluxes through sulfate

146 reduction in sediments (Raymond et al., 2000; Najjar et al., 2020). Ω_{Ca} is calculated from DIC, TA, temperature, and salinity

147 using CO2SYS (van Heuven et al., 2011) using the equilibrium constants of Cai and Wang (1998) as they are suitable for both

148 fresh and estuarine waters (Dinauer and Mucci, 2017; Herrmann et al., 2020). Although submerged aquatic vegetation is a

149 possible source of $CaCO_3$ (Mazarrasa et al., 2015; Su et al., 2020), $CaCO_3$ precipitation and dissolution are not simulated in

150 ECB due to both insufficient observations and low submerged aquatic vegetation presence throughout the model domain (Orth

151 et al., 1998; Moore et al., 2009).

152   Several additional updates have been made in this implementation of ROMS-ECB to better represent oxygen and

153 primary production dynamics in the lower Virginia tributaries. The maximum phytoplankton growth rate has been increased

154 to 2.15 d^{-1}, and the growth rate is limited in the fresh portion of the tributaries using a Michaelis-Menten function of salinity

155 and a half-saturation of 1.5 (Da et al., 2024). The sediment bed climatology from Moriarty et al. (2021) has been adjusted to

156 better represent the sand class distributions published in Nichols (1991) and observations taken by the USGS (Reid et al.,

157 2005). Specifically, the changes include a greater percentage of small clay-rich flocs throughout the main stem of the York

158 River as well as more sand and large silt-rich flocs in the Rappahannock River. Previously, the sediment module assumed the

159 same critical shear stress for large silt-rich flocs, small clay-rich flocs, and unaggregated mud; here, the critical shear stress of

160 smaller particles is lower than larger particles, meaning smaller particles resuspend more easily. The updated critical shear

161 stress coefficient for erosion and deposition is 0.5 Pa for large silt-rich flocs and 0.4 Pa for both small clay-rich flocs and

162 unaggregated mud, which represent a small portion of the sediment bed. The ballasting formulation of Turner et al. (2021) has
163 also been added to simulate the increase in particle sinking rates due to the aggregation of particles in turbid waters.

2.1.3 Oyster bioenergetics model

165   As part of this study, the oyster bioenergetics model EcoOyster (Brush and Kellogg, 2018; Kellogg et al., 2018) has
166 been one-way coupled to ROMS-ECB in the deepest (bottom) level (see Supplementary Tables S1-S4 for EcoOyster
167 equations). The one-way coupling means that environmental conditions from ROMS-ECB influence oyster growth in
168 EcoOyster, but the oysters do not influence water quality conditions in ROMS-ECB. This allows the focus of our analysis to
169 be on the effect of future climate change on oyster growth, rather than the effect of oyster growth on water quality, which has
170 been previously studied in the Chesapeake Bay (e.g., Gawde et al., 2024). By focusing on the deepest vertical level of the
171 model, the assumption is that oysters are growing on the bottom, and not inside floating cages. This is representative of
172 conditions similar to on-bottom or bottom cage aquaculture methods that are common in Virginia. The coupled model, referred
173 to hereafter as ROMS-ECBO, simulates daily somatic tissue dry weight, gonadal tissue dry weight, shell dry weight, and shell
174 height of diploid and triploid oysters as a function of filtration, respiration, egestion, allocation to reproduction, calcification,
175 and dissolution (Brush and Kellogg, 2018; Kellogg et al., 2018; Rivest et al., 2023). For the purpose of this study, only diploid
176 oysters were included, as model equations were developed from a study on diploid oysters, and triploid allometric equations
177 are not as well constrained. Tissue growth rates depend on individual weight together with temperature, salinity, O_2, TSS, and
178 POC from ROMS-ECB. Chl$a$ is required for the filtration function and is calculated from ROMS-ECB phytoplankton carbon
179 and Kd, in combination with seasonal carbon:chl$a$ ratios that are computed using equations from Cerco and Noel (2004). The
180 calcification function includes a threshold value of $\Omega_{Ca} = 0.93$, determined through laboratory experiments with Eastern oysters
181 (Rivest et al., 2023).

182   The *EcoOyster* equations were developed from a meta-analysis of existing oyster bioenergetics models and laboratory
183 experiments with diploid oysters (Brush and Kellogg, 2018; Kellogg et al., 2018; Rivest et al., 2023). Allometric relationships
184 between shell dry weight, tissue dry weight, and shell height used for initial conditions were derived from observational data
185 in the Chesapeake Bay (VOSARA, 2024). Total dry tissue weight is calculated as the sum of somatic tissue weight and gonadal
186 weight. Reproduction is simulated through gonadal weight, a function of growth of gonadal tissue, resorption of gonadal tissue,
187 and spawning (Hofmann et al., 1994). Somatic tissue weight is a function of assimilation, respiration, growth of gonadal tissue,
188 and resorption of gonadal tissue. Assimilation is a function of filtration and POC. Filtration is a function of a maximum
189 filtration rate based on tissue weight, limited by sub-optimal temperature, salinity, TSS, O_2, and chl$a$ (Cerco and Noel, 2005;
190 Fulford et al., 2007; Ehrich and Harris, 2015). The optimal temperature for oyster filtration (T_{opt}) is set to 27 °C (Jordan, 1987).
191 Filtration is also multiplied by p, a tunable factor representing the proportion of computed filtration actually performed by
192 oysters, which accounts for processes excluded from the model such as time spent filtering and is constrained by published
193 growth rates. Respiration is a function of tissue weight, temperature, and assimilation. While filtration has a temperature
194 limitation, respiration increases exponentially with temperature (Fig. S1). Tissue growth functions are not affected by

195 carbonate chemistry variables, as experimental studies have found that neither filtration (Lemasson et al., 2018) nor respiration
196 (Beniash et al., 2010; Matoo et al., 2013) of oysters are affected by pH changes; however, weight-specific net calcification is
197 a function of Ω_{Ca} and temperature (Rivest et al., 2023). Shell growth is a function of both total tissue weight and net
198 calcification.

2.2 Present day reference simulation

200   A realistic reference simulation was generated to represent 2017 conditions. The year 2017 was chosen for
201 atmospheric, terrestrial, and open-ocean boundary conditions as this represents a relatively typical hydrological year.
202 Atmospheric forcings (air temperature, long- and short-wave radiation, precipitation, winds, dewpoint temperature, and air
203 pressure) are obtained from the ERA5 atmospheric reanalysis (Copernicus Climate Change Service, 2017; Hersbach et al.,
204 2020). Surface atmospheric variables are available at 3-hourly intervals with a 0.25° resolution and are interpolated to a 0.2°
205 grid. Terrestrial inputs of freshwater, nitrogen, carbon, and sediment are derived from the Phase 6 CBP Watershed Model
206 (CBPWM; Bhatt et al., 2023) and USGS data. Daily estimates of freshwater discharge, water temperature, and loadings of
207 nitrate, ammonium, organic nitrogen, and four classes of sediment from the CBPWM were concatenated to 74 locations
208 throughout the model domain. To compute carbon loadings, constant carbon-to-nitrogen ratios are used, specifically 10:1 for
209 dissolved organic matter (Hopkinson et al., 1998) and 6.625:1 for particulate organic matter (Redfield, 1934). Riverine TA
210 concentrations are computed as in Da et al. (2024), using monthly-varying linear relationships between historical USGS
211 observations of discharge and USGS TA estimates determined using the Weighted Regression on Time, Discharge, and Season
212 (WRTDS; Hirsch et al., 2010) approach. Riverine DIC is calculated from daily riverine TA and daily DIC:TA ratios, linearly
213 interpolated from the monthly climatology of USGS WRTDS DIC:TA in each tributary. Open boundary conditions are derived
214 from a recent 600 m resolution whole-bay implementation of ROMS (St-Laurent and Friedrichs, 2024). Initial conditions for
215 the six-month spin-up were derived from Da et al., (2024).

216   Since spring-spawned oysters are typically deployed in late spring through summer on oyster farms, the reference run
217 was started on July 1st and spanned one full year, ending June 30th of the following year. Oyster sizes were initialized based
218 on shell height approximations of a typical spring-spawned oyster at deployment in July (i.e., a few months old). Starting dry
219 tissue weight was assumed to be 0.001 g for all oysters, back-calculated from the approximate height of an oyster at the time
220 of deployment. Starting shell dry weights and heights were calculated from allometric relationships to be 0.144 g and 11.6
221 mm, respectively.

2.3 Comparison of reference simulation to in situ observations

223   *In situ* water quality monitoring observations are available since 1984 throughout the Chesapeake Bay. Specifically,
224 the Chesapeake Bay Program's Water Quality Monitoring Program (CBP WQMP) conducts cruises in the Bay and its
225 tributaries. On average, stations are sampled once monthly, with the exception of June through August in the mainstem, when
226 sampling occurs twice. In this study, measurements of water temperature, salinity, O_2, pH (NBS scale), TSS, and POC are

227 used from 16 CBP stations throughout the model domain, with depths ranging from 5 to 16 m (Fig. 1a; CBP, 2024). For all

228 variables except TSS and POC, measurements are taken *in situ* using a YSI or Hydrolab® sonde roughly every one to two

229 meters of the water column. TSS and POC are obtained from bottle samples at the surface, bottom, and at deeper stations, two

230 additional depths above and below the pycnocline. TSS is determined by filtering a known volume of water through a pre-

231 weighted filter and then re-weighing the filter after filtration and drying. POC is determined through combustion of a filter

232 using an elemental analyzer (Olsen, 2012).

233 Model skill was evaluated by comparing results from the reference simulation to the CBP WQMP observations

234 described above. Hourly outputs from the four closest grid cells to each CBP station were spatially interpolated to obtain results

235 at each respective station. Multiple variables in ECB at the bottom level of the model, including temperature, salinity, O_2, pH,

236 TSS, and POC, were compared with observations from the same station and time, within the bottom 10% of the water column

237 (Table 1). Model bias and root-mean squared difference (RMSD) were computed for all aforementioned variables. Seasonal

238 skill was also evaluated by comparing the 2017 reference run to CBP decadal averages. Decadal means were used for these

239 comparisons, as once-monthly or once-seasonally sampling dates in 2017 bias outputs toward conditions on the time of the

240 month when the measurements were taken in 2017, and the purpose of the comparison was to examine how the model

241 reproduces average seasonal variability.

2.4 Future simulations

243 In addition to the reference run, this study generated five future simulations (Table 1) to investigate the change in

244 carbonate chemistry conditions and oyster growth resulting from three drivers of future change in the bay: increased

245 atmospheric CO_2 (*AtmCO$_2$*), atmospheric warming (*Temp*), and reduced nutrient loading (*TMDL*). Model forcings were

246 modified for each simulation to represent mid-century conditions. A *Combined Future* simulation was run including forcings

247 of all future stressors, in addition to three sensitivity simulations to isolate the impacts of each stressor on oyster growth.

248 Atmospheric CO_2 concentration for the *AtmCO$_2$* and *Combined Future* simulations was set to 655 ppm, derived from the

249 Coupled Model Intercomparison Project Phase 5 report RCP8.5 (business-as-usual) scenario projected for 50 years in the

250 future relative to the reference run (Meinshausen et al., 2011). While it is reasonable to assume that warming temperatures will

251 always accompany increases in atmospheric CO_2, separate experiments for each stressor were conducted. Isolating the

252 physiological effects of each stressor helps us understand the mechanisms effecting the change in oyster growth and

253 furthermore indicates the degree to which management strategies for offsetting acidification can reduce the effects of climate

254 change on oysters. Future atmospheric temperature for the *Temp* and *Combined Future* simulations was obtained from the

255 IPSL-CM5B-LR Earth System Model (Dufresne et al., 2013), statistically downscaled with the Multivariate Adaptive

256 Constructed Analogs method (Abatzoglou and Brown, 2012). IPSL-CM5B-LR was selected as in Hinson et al. (2024), since

257 it was deemed the most representative downscaled ESM of the 20 available (Hinson et al., 2023). As in Hinson et al. (2024),

258 the delta method was used to calculate the daily average change in atmospheric temperatures between present-day and future

259 conditions. To calculate this change, two 30-year climatologies, centered on 2000 and 2050 respectively, were computed and

daily averaged 50-year differences between the two climatologies (Fig. 2) were added to the atmospheric temperatures used in the reference run. Future watershed inputs for the *TMDL* and *Combined Future* simulations included a climatology of nitrate, ammonium, dissolved organic matter, and particulate organic matter concentrations, derived from a Phase 6 CBPWM 1991-2000 run using reduced nutrient concentrations assuming the TMDLs had been successfully achieved (approximately a 20-25% mean reduction in total nutrient loading; Bhatt et al., 2023). Freshwater discharge in this run was set to be identical to the reference run, to isolate the effects of lowered nutrient concentrations on water chemistry and oyster growth. Since future climate change is expected to impact terrestrial inputs much less than future management actions (Hinson et al., 2023), the direct impact of climate change on the watershed is not considered in this analysis. A fifth simulation (*AtmCO$_2$ + Temp)* was run to compare the influences of local management actions to the combined drivers of climate change, which includes both future atmospheric CO_2 concentration and atmospheric temperature. Preliminary investigations revealed a minimal impact of sea level rise on Ω_{Ca} in the bay; therefore, it was not included in the simulated climate change variables.

To generate open boundary conditions for each future simulation, a full bay model (St-Laurent and Friedrichs, 2024) was run with the same atmospheric and river forcings as in this 120-meter model implementation. As in the reference run, all future simulations were spun up for six months (January 1 – June 30) before beginning on July 1, but represent 50 years in the future from the reference simulation (i.e., July 1, 2067). Initial conditions for all spin-ups are identical to the reference simulation. Analysis confirmed the effects of initial conditions are negligible by July 1. To examine results most relevant to oysters, model output was extracted at locations that support oyster production, defined as all grid cells in which tissue weight exceeded 1 g at the end of the reference run (i.e., one year of growth; Fig. S2), which is inclusive of locations of active oyster farms. All results shown are from the bottom level of the model, representing conditions similar to on-bottom or bottom cage aquaculture methods that are common in Virginia. Spatial variation in model outputs across grid cells in the model domain is reported using standard deviation.

3 Results

3.1 Model Skill Assessment

When compared to 2017 WQMP observations and seasonal decadal averages, model skill of ROMS-ECB is reasonably high (Table 2, Figs. 3, 4), and similar to other model implementations of the Chesapeake Bay (Irby et al., 2016). Temperature and salinity are reproduced relatively well year-round (Fig. 3a,b) with annual biases of only 0.2°C and -1.5, respectively (Table 2). Bottom O_2 and pH are slightly overestimated, exhibiting the greatest model-data misfit in the spring and summer months in the tributary channels (Fig. 3c,d). pH is overestimated by 0.2 units, which is within the accuracy of the electrode measurements. Observed POC concentrations in the York and upper Rappahannock are higher than simulated in the model and exhibit very high spatial variability (Fig. 4a). Despite the high spatial variability of the TSS observations (Fig. 4b), mean TSS (45 ± 54 mg L^{-1}) is captured within 1.1 mg L^{-1} by the model.

291   Growth rates determined using the *EcoOyster* equations and environmental outputs from ROMS-ECB were compared
292 with oyster data collected in the York River (Paynter et al., 2008; Liddel, 2008; Kingsley-Smith et al., 2009; Degremont et al.,
293 2012; Callam et al., 2016). Specifically, the tunable parameter (p) that limits oyster filtration was adjusted to provide a best
294 match between the modeled oyster growth rates and the published rates. Multiple p-values were tested, and a value of p=0.15
295 resulted in modeled oyster growth that best matched published growth rates. The resulting shell growth predicted by the model
296 was found to be close to the *in situ* data (52.0 ± 1.1 mm y^{-1} and 51.3 ± 2.9 mm y^{-1} for the model and observation means and
297 standard deviations, respectively).

3.2 Reference run results

299   In the present-day reference run, the environmental variables used as inputs to the oyster parameterizations exhibit
300 substantial seasonal (Fig. 5a-f) and spatial (Figs. 6, S3) variability. As expected, bottom temperature is highest in summer,
301 reaching an average of 29.3 °C in July when averaged across grid cells that support oyster growth (Fig. 5a). Temperature is
302 higher in the shallower parts of the tributaries compared to the channels (Fig. S3a). Bottom salinity exhibits higher values in
303 the fall and winter, reaching a maximum average of 17.7 in October, and drops in the spring and summer to reach a minimum
304 average of 12.3 in June (Fig. 5b). Annual average bottom salinity ranges from 0 to 26 throughout the model domain (Fig. S3b),
305 with the highest values in the southern areas in closest proximity to the open-ocean. The seasonal cycle for bottom POC is
306 similar to that of temperature, peaking at 1.7 g C m^{-3} in June and dropping to 0.57 g C m^{-3} in January (Fig. 5c). Bottom POC
307 also varies widely throughout the model domain (Fig. 6a), with relatively higher values in the Rappahannock compared to the
308 York River, along the shoals of the tributaries, and along the western shoals of the mainstem Bay north of the Rappahannock.
309 Ω_{Ca} exhibits an annual cycle similar to that of temperature and POC, reaching a maximum average of 3.2 in August and a
310 minimum average of 1.1 in January (Fig. 5d). Annual mean bottom Ω_{Ca} also varies widely throughout the model domain (Fig.
311 6d). Generally, bottom Ω_{Ca} increases with salinity, with low to zero values in the tidal fresh portions of the upper tributaries
312 and higher values along the western shoals of the mainstem Chesapeake Bay. The opposite temporal pattern is seen in bottom
313 O$_2$, which peaks at 12.3 mg L^{-1} in February and drops to an average of 6.3 mg L^{-1} in August (Fig. 5e). O$_2$ concentrations are
314 highest along the shoals and lowest in the deep channels (Fig. S3c). Bottom TSS concentrations exhibit tidal variability
315 throughout the year and are highest in the York River with much lower concentrations observed in the other portions of the
316 model domain (Fig. S3d).
317   Tissue and shell weights increase modestly from July through April, and the highest rates of increase are seen in May
318 and June near the end of the one-year reference run (Fig. 5g,h). At the end of the reference run, the spatial patterns of shell and
319 tissue weight are nearly identical (Fig. 7), as tissue growth largely drives shell growth (Table S4). Both shell and tissue weights
320 are highest along the shoals of the York and Rappahannock Rivers (Fig. 7a,d) and low in the deeper waters where TSS
321 concentrations are high (Fig. S3d). A wider region of high shell and tissue weight appears in the Rappahannock, while the
322 highest weights in the York are confined to a very narrow and shallow strip along the coastline. Shell and tissue weights are

323   higher along the southwestern than the northeastern coastlines of the tributaries, where the shoals are wider in both tributaries

324   (Fig. 1a).

325   **3.3 Results of Combined Future simulation**

326   All environmental variables examined exhibit change from the reference run in the *Combined Future* simulation.

327   Temperature and salinity are projected to increase across the entire model domain (Fig. S3a,b). When averaged over the model

328   domain, temperature is projected to increase by 1.5 ± 0.26°C, and salinity is projected to increase by 0.21 ± 0.11 (Table S5).

329   Bottom POC is projected to decrease by 0.07 ± 0.05 g C m^3 (Table S5), with POC reductions predicted to be most pronounced

330   in the mid- to upper tributaries (Fig. 6c). Mid-century bottom Ω_{Ca} is projected to be lower throughout most of the region (Fig.

331   6f), with an average reduction of 0.8 ± 0.19 over the whole model domain (Table S5). The spatial distribution of future Ω_{Ca} is

332   generally consistent with present-day Ω_{Ca} patterns, and the greatest decreases are projected to occur in regions with the highest

333   present-day Ω_{ca} (Fig. 6 d,e,f). An average reduction in O_2 of 0.3 ± 0.08 mg L^{-1} is predicted across the model domain (Table

334   S5), which will be mostly spatially uniform (Fig. S3c). TSS is projected to be reduced by 0.20 ± 0.25 mg L^{-1} with high spatial

335   variability in the projected change (Table S5; Fig. S3d).

336   Changes in environmental conditions do not occur uniformly throughout the year. Temporal changes in environmental

337   conditions averaged across grid cells that support oyster growth are provided in Figure 5. Annually averaged increases in

338   temperature and salinity are the same when averaged over only grid cells that support oyster growth as they are when averaged

339   across the entire model domain (Tables 3, S5). The greatest temperature increases are projected to occur in the warmer months,

340   with an average increase of 1.6 °C predicted for June through August and an average increase of 1.2 °C predicted for December

341   through February. Bottom temperatures are projected to surpass the optimal temperature for oyster filtration (27 °C) primarily

342   in July and August (Fig. 5a). Salinity increases are projected to be greatest at the beginning of the year, with an average increase

343   of 0.44 between January and March and an average increase of 0.20 for the remainder of the year (Fig. 5b). Bottom POC at

344   grid cells that support oyster growth is expected to decrease slightly less than the average for the entire region (Tables 3, S5),

345   by an annual average of 0.09 g C m^{-3}, with the greatest reductions in the spring and summer and little to no change in the

346   winter (Fig. 5c). For Ω_{Ca}, O_2, and TSS, projected reductions are slightly greater at oyster growth sites than for the entire domain.

347   Ω_{Ca} is projected to decrease by 0.9, with the greatest reductions expected to occur the warmer months (Fig. 5d). O_2 is projected

348   to decrease year-round, though with slightly greater reductions in the winter (Fig. 5e) and an annual average reduction of 0.4

349   mg O_2 L^{-1} (Table 3). TSS is projected to decrease annually by 0.3 mg L^{-1} (Table 3), mostly in the spring, due to lowered POC

350   (Fig. 5f).

351   Modeled shell and tissue weights after one year of growth are projected to decline in all regions that exhibit present-

352   day growth, with the most severe reductions (up to 100%) occurring along the York and Rappahannock River shoals (Figs.

353   7c,f, 8). One-year tissue weight will be reduced by 1.3 g, on average, representing a 60% reduction across grid cells that support

354   oyster growth (Table 4). Shell weight, which is largely driven by changes in tissue weight, is projected to be reduced by 11.4

355   g on average after one year of growth, representing a 68% reduction in average shell weight in regions that support oyster

growth (Table 4). The greatest reduction in shell and tissue growth rates will occur in the warmer months near the end of the one-year simulation (-0.1 g d^{-1} from May through June), whereas the smallest change will occur in the winter months (-0.02 g d^{-1} from December through February), as the least growth occurs during that time (Fig. 5g,h). Shell thickness, calculated as the ratio of shell weight to shell height, will be reduced by 61% on average (0.11 g mm^{-1}; Table 4).

Declines in year one shell weight will vary throughout the model domain (Fig. 8), following relative changes in bottom POC and Ω_{Ca} (Fig. 9). The mainstem has the most moderate reduction in shell weight relative to reference shell weight, with an average reduction of 31%, indicated by the slope of the scatterplot. Shell weights in the Rappahannock and York face the steepest reductions relative to reference, with average reductions of 86% and 96%, respectively, and a large portion of York oysters facing complete depletion of oyster tissue and shell in these locations (Fig. 9; indicated by proximity to 1:1 line). Proportional shell weight reductions in the mainstem are projected to correlate with POC reductions (Fig. 9a). For Ω_{Ca} in the mainstem, a group of sites face the greatest proportional reductions when Ω_{Ca} reductions are the greatest. However, for sites with lower proportional shell loss, the opposite trend is observed (Fig 9d). In the Rappahannock, higher POC reductions coincide with slightly lower proportional shell loss (Fig. 9b). Sites with the largest reductions in POC primarily occur in the York (Fig. 9c; see dark blue symbols on the 1:1 line), and the greatest proportional shell weight reductions coincide with the greatest POC and Ω_{Ca} reductions (Fig. 9c,f). Similar results are found for tissue weight (not shown).

3.4 Results of individual future sensitivity simulations

Four individual future sensitivity simulations were conducted to isolate the specific mechanisms (increased atmospheric CO_2, increased atmospheric temperature, and/or nutrient reductions) causing the projected changes described above in the *Combined Future* simulation. The *AtmCO₂* sensitivity simulation produces substantial reductions in average bottom Ω_{Ca} (Fig. 10d) and, as expected, is not projected to substantially impact bottom temperature, salinity, POC, O_2, or TSS (Table 3; Figs. 10a, S4). The projected reduction in Ω_{Ca} is 0.9 when averaged over oyster growth sites (Table 3), 0.1 greater in magnitude than the average reduction for the entire model domain (Table S5), as greater reductions are expected along the shoals of the Rappahannock and mainstem shoal than the York and upper section of the Rappahannock (Fig. 10d). In this *AtmCO₂* simulation, shell weight is predicted to be most steeply reduced in the Rappahannock, with less impact in the York and mainstem regions (Fig. 11a). At grid cells with oyster growth, *AtmCO₂* produces a shell weight reduction of 6.3 g and a shell thickness reduction of 0.06 g mm^{-1} in comparison to the reference simulation, but no change in tissue weight (Table 4).

The *Temp* sensitivity simulation produces changes in all environmental variables impacting oyster growth, with the exception of Ω_{Ca} (Tables 3, S5). Average changes in temperature, salinity, and TSS will be identical to those from the *Combined Future* simulation (Tables 3, S5). Predicted reductions in POC and O_2 will be smaller in magnitude than in *Combined Future,* though more severe than any other single sensitivity experiment (Table 3, S5). Temperature and salinity will increase across the entire model domain, with a greater salinity increase occurring in the Rappahannock and along the mainstem shoal (Fig. S4a-c). TSS will decrease primarily in the channels of the lower York and Rappahannock and on the mainstem shoal (Fig. S4d). POC reductions are expected to cover the majority of the model domain, with larger reductions in

the upper Rappahannock (Fig. 10b). Slight increases in Ω_{Ca} are observed in shallow tidal creeks (Fig. 10e); however, no substantial change in average Ω_{Ca} is predicted (Table 3, S5). O_2 at oyster grid cells will exhibit a similar but slightly smaller average reduction compared to *Combined Future* (Table 3). Patterns of change in shell weight in the *Temp* sensitivity simulation resemble those in the *AtmCO2* simulation (Figs. 7c, 11b), with additional reductions along the mainstem shoal and a greater predicted mean reduction of 7.1 g, a 42% decrease at grid cells with oyster growth (Table 4). Unlike *AtmCO2*, tissue weight will decrease in *Temp*, by an average of 1 g, a 46% reduction (Table 4).

The *TMDL* sensitivity simulation produces a much smaller average change in environmental conditions than the *AtmCO2* or *Temp* simulations (Tables 3, S5). *TMDL* does not substantially influence temperature, salinity, or O_2 (Tables 3, S4, S5), but produces POC and TSS reductions close to the averages for *Temp* (Tables 3, S5). While POC change in the *Temp* simulation is concentrated in the deeper portions of the tributaries (Fig. 10b), the POC reductions in the *TMDL* simulation are concentrated along the shoals of the tributaries, with the greatest reductions in the upper Rappahannock (Fig. 10c). TSS changes in *TMDL* are limited to the tributaries, occurring along the shoals of the Rappahannock and in patches throughout the York (Fig. S4d). Future change in Ω_{Ca} in this simulation is less than for *AtmCO2* and is largely confined to the upper Rappahannock shoals and in shallow tidal creeks throughout the study region (Fig. 10d, f). Patterns of change in shell weight will resemble *AtmCO2* and *Temp* in the tributaries, but no change is predicted along the mainstem shoal (Fig. 11a-c). The *TMDL* simulation produces reduced shell (3.7 g) and tissue (0.5 g) weights, with a smaller negative influence on shell and tissue weight than *Temp* (Table 4; Fig. 11b-f).

Environmental conditions in the *AtmCO2 + Temp* simulation are nearly identical to those in the *Temp* simulation (Tables 3, S5), with the exception of Ω_{Ca}, which is lower due to the influence of heightened atmospheric CO_2. As tissue growth is unaffected by Ω_{Ca}, tissue weight in this simulation is identical to that of the *Temp* simulation (Table 4). Average shell weight reduction in *AtmCO2 + Temp* is 10.2 g, greater than that from *AtmCO2* alone, due to the combined influences of lowered tissue growth and lower Ω_{Ca} (Table 4).

4 Discussion

This study provides high-resolution projections for oyster growing conditions and corresponding oyster growth in the Chesapeake Bay, with a specific focus on two Virginia tributaries. A high-resolution hydrodynamic-biogeochemical model was coupled with an Eastern oyster bioenergetics model and forced with future projections for atmospheric CO_2, temperature, and nutrient management. An overall reduction in Ω_{Ca} and oyster growth are predicted by mid-century throughout the study region under the combined effects of all three future stressors. Specifically, the greatest reductions in oyster growth are projected to occur in the York and Rappahannock Rivers, where unfavorable conditions for calcification will expand in the future and where food availability will be strongly impacted by warming and nutrient reductions. Bottom conditions in the York and Rappahannock rivers, particularly in the upper portions, will likely be unsuitable for aquaculture at mid-century on average, indicating climate change preparedness is critical for the oyster aquaculture industry.

4.1 Future projections of Ω_{Ca}

421

422   The magnitude of future change in Ω_{Ca} varies with present-day Ω_{Ca} conditions (Fig. 6d-f). Regions with high present-
423 day Ω_{Ca}, primarily the mainstem shoals, are projected to experience the greatest reductions because of their low partial pressure
424 of CO_2 (pCO_2) relative to fresher waters. Biologically driven low pCO_2 water on mainstem shoals has a greater capacity for
425 CO_2 uptake from the atmosphere than high pCO_2 water, which is causing the fresher tributaries to experience smaller increases
426 in DIC and smaller reductions in Ω_{Ca} (Fig. 6f). Acidic freshwater input often causes pCO_2 in the upper tributaries to exceed
427 atmospheric pCO_2, causing outgassing (Cai et al., 2017; Shen et al., 2019b; St-Laurent et al., 2020; Cai et al., 2021). Despite
428 the lower Rappahannock having a lower salinity than the lower York, it also has a lower DIC to TA ratio, so the rate at which
429 the lower Rappahannock absorbs pCO_2 is higher (Da et al., 2021). Total alkalinity, or buffering capacity, is also lower in the
430 lower Rappahannock than the lower York (Da et al. 2021), so the lower Rappahannock cannot resist changes in carbonate
431 chemistry to the same degree as the York. As a result, we observe the Rappahannock changing faster than the York (Fig.6f,
432 Fig. 9). Since higher Ω_{Ca} regions will experience greater reductions than lower Ω_{Ca} regions (Fig. 6d-f), the overall spatial
433 variability of Ω_{Ca} will be reduced by mid-century, and more areas will experience conditions that are unfavorable for oyster
434 shell-building (Fig. 5).

435   Although future atmospheric CO_2 and reduced nutrient loading will both contribute to Ω_{Ca} reductions, the modeling
436 experiments conducted here highlight that increasing atmospheric CO_2 is the largest contributor to decreases in Ω_{Ca} throughout
437 the study region. Increased atmospheric CO_2 will cause reductions in Ω_{Ca} across the model domain, while nutrient reductions
438 are expected to mainly influence Ω_{Ca} in shallow and fresh coastal areas, with little influence in oyster growing regions. The
439 effects of warming on Ω_{Ca} may slightly offset the influence of atmospheric CO_2 in certain areas, but this will likely only occur
440 in fresh tidal creeks where oysters do not currently reside (Fig. 10e). Given the importance of atmospheric CO_2 in shaping
441 future Ω_{Ca} conditions in the lower bay, reductions in anthropogenic carbon emissions will be necessary to lessen the projected
442 impacts on carbonate chemistry in the Chesapeake Bay and globally.

443   Comparing our results to other studies examining the effects of acidification reveals that the Chesapeake Bay will
444 likely acidify faster than the US West Coast. Siedlecki et al. (2021a) projected a decrease of 0.8-1.0 in Ω_{Ca} in the Northern
445 California Current System between 2000 and 2100 under the same future emissions scenario used in our study, i.e., RCP8.5.
446 Projections from the present work indicate a similar magnitude of reduction in the lower Chesapeake Bay over a shorter time
447 period (50 years), suggesting a faster rate of acidification in the lower bay. Feely et al. (2009) also reported that projections
448 for Ω_{Ca} reductions are slightly greater in the Atlantic than in the Pacific. The relative differences in rates of acidification should
449 be considered, however, in the context of present-day Ω_{Ca}. The Pacific Ocean has a higher ratio of DIC:TA than the Atlantic,
450 so present-day Pacific Ω_{Ca} is lower (Feely et al., 2004; Dunne et al., 2012). Therefore, while the Chesapeake Bay is acidifying
451 faster, coastal Pacific waters may become undersaturated with calcite and aragonite sooner than in Chesapeake Bay. US West
452 Coast shellfish mortality events associated with acidification or other climate change stressors may place increased pressure
453 on US Atlantic fisheries to provide shellfish to the nation, highlighting the importance of climate change preparedness and
454 resilience in the Chesapeake Bay region.

455   While atmospheric CO_2 is primarily responsible for changes in Ω_{Ca}, nutrient reductions are also projected to worsen
456   carbonate chemistry conditions. Eutrophication can suppress acidification in surface waters by increasing primary production
457   (Borges and Gypens, 2010; Shen et al., 2019; Da et al., 2021), and when simulating a reduction in eutrophication via nutrient
458   management in our modeling study, the countering effect occurred. While the reduction in Ω_{Ca} from nutrient management is
459   minor compared to the projected impacts of CO_2-driven acidification, its small contribution may shift Ω_{Ca} conditions from
460   favoring net calcification to favoring net dissolution, demonstrating the importance of considering multiple drivers when
461   predicting exposure to ecologically relevant conditions of coastal acidification.

462   **4.2 Future projections of oyster growth**

463   Acidification, warming, and nutrient reductions are projected to affect shell and tissue growth of oysters in different
464   ways. Here, increased atmospheric CO_2 caused reductions in shell growth of Eastern oysters due to its negative effect on Ω_{Ca}
465   and thus calcification rates, which is consistent with experimental studies (Waldbusser et al., 2011; Gobler and Talmage, 2014;
466   Himes et al., 2024). Shell weight reductions from increased atmospheric CO_2 were driven by changes in calcification rate
467   alone, as tissue weight in *EcoOyster* is unaffected by Ω_{Ca} (Fig. 11d; Rivest et al., 2023). Experimental studies have identified
468   indirect physiological impacts of elevated CO_2 on juvenile/adult oyster metabolism, growth, and reproduction (Beniash et al.,
469   2010; Dickinson et al., 2012), suggesting that increased atmospheric CO_2 can sometimes influence tissue growth. Further
470   investigation is necessary in order to include the relationship between atmospheric CO_2 and oyster tissue growth in *EcoOyster*.
471   Biological and chemical reactions occur faster at higher temperatures, meaning calcification rates may be higher under future
472   warming conditions (Waldbusser et al., 2011), as long as Ω_{Ca} is still high enough to support calcification. Conversely, under
473   conditions of extreme low Ω_{Ca}, warming may exacerbate dissolution rates and shell weight reductions. Our results also show
474   that nutrient reductions will lead to reductions in shell weight, largely driven by a reduction in tissue weight resulting from
475   lower food availability (POC), rather than lower Ω_{Ca}.

476   While nutrient reductions are projected to have little influence on Ω_{Ca} in this study, their negative influence on food
477   availability may be detrimental to tissue growth in certain parts of the study region, particularly the York River. Our model
478   projections suggest that nutrient reductions may in some cases produce conditions that do not support any oyster growth along
479   the shoals of the York (Fig. 9c, f), a result of reductions in food availability that are predicted to be more substantial in the
480   tributaries than the mainstem region (Fig. 10c). Multiple studies have demonstrated that Eastern oysters and other calcifying
481   organisms perform better under acidification when they have sufficient food availability, as they are better able to keep up
482   with the energetic demands of environmental stress (Thomsen et al., 2015; Ramajo et al., 2016; Schwaner et al., 2023, Caillon
483   et al., 2025). Therefore, nutrient reductions will likely influence oyster growth under acidification stress by different
484   magnitudes in each tributary. When comparing the effects of local management actions to reduce nutrient runoff to the effects
485   of climate change (increased atmospheric CO_2 and warming), it is evident that, on average, climate change will have a much
486   greater negative influence on oyster growth (Table 4). However, the strong localized impacts of nutrient reductions in the York

highlight the importance of examining the spatial variability of future changes in oyster growth. It is important for managers to consider local conditions when assessing the effects of nutrient reductions on oyster production.

Increased water temperatures are projected to slow oyster growth in the future. Specifically, large reductions in tissue weight are underpinned by three primary mechanisms: limitations on filtration at high temperatures (Loosanoff, 1958), increased respiration rates (Dame, 1972), and reduced food availability. In *EcoOyster,* the optimal temperature for Eastern oyster filtration is 27°C (Cerco et al., 2005; Jordan, 1987), and under warming, the frequency at which ambient summer temperatures will surpass this optimal temperature will be higher (Fig. 5a), therefore causing more frequent declines in filtration rate (Cerco et al., 2005; Fulford et al., 2007). There is no clear optimal temperature for oyster respiration, and therefore it is assumed to increase exponentially with temperature (Hochachka and Somero, 2002). Thus, as oyster filtration rates begin to decline at high temperatures, respiration rates will continue to rise and decrease the potential for tissue accumulation (Fig. S1). Previous studies on juvenile Eastern oysters do not support a consensus on the relationship between warming and tissue growth. Some report that growth is inhibited at higher temperatures (31°C, Stevens and Gobler, 2018; 30°C, Speights et al., 2017). In contrast, Talmage and Gobler (2011) found no significant influence of high temperature (28°C) alone on tissue growth. The optimal temperature for oyster filtration may also vary among oysters, based on observations of maximum filtration rates of adult Eastern oysters occurring between 28.1°C– 32°C (Loosanoff, 1958). Variation in experimental design may have contributed to the contrast in results summarized here, in addition to the influence of local adaptation (Burford et al., 2014). Other studies that incorporate higher temperature thresholds into their models predict increases in oyster biomass under warming in Chesapeake Bay (Allen et al., 2023), underscoring the importance of properly parameterizing growth models. Additional modeling studies should be conducted to test the sensitivity of oyster growth changes to optimal temperature parameterizations. Due to a lack of consensus on temperature limits of Eastern oyster filtration, further research is also needed to more robustly represent oyster filtration in bioenergetics models and improve predictions of impacts of warming on oysters and their ecosystem services in the region.

Warming will likely have a negative effect on food availability for oysters. Compared to the effects of nutrient reductions, warming will have a much more widespread influence on POC, causing reductions throughout the model domain (Fig. 10b,c). Despite warming increasing rates of POC production via increased phytoplankton growth rates, factors such as nutrient limitation and increased respiration rates will result in a net decrease in POC availability. In the tributaries, reductions in food availability will be most widespread due to warming, but less extreme than those from nutrient reductions in the shallow parts of the tributaries where oysters are affected. Remineralization of organic carbon in marine systems is temperature-dependent (López-Urrutia et al., 2006), and as warming occurs, remineralization of detrital carbon to DIC in bottom waters will occur at higher rates. As much of the lower bay is nutrient-limited (Zhang et al., 2021), phytoplankton growth rates will not increase much from warming alone; therefore, increased remineralization will likely reduce the overall amount of food available to oysters. Despite a similar average reduction in food availability being predicted for the future warming simulation and managed nutrient reductions simulation, the influence of warmer temperatures will amplify the negative effects of reduced food availability on growth. In this study, the critical temperature at which respiration rates exceed assimilation rates is

dependent on filtration. When food availability limits filtration, this critical temperature lowers, and the temperature threshold for tissue loss is lowered. Experimental studies have demonstrated how organic carbon may be influenced by both warming and acidification (Simone et al., 2021), but as these dynamics can differ based on nutrient availability, it is important to consider how climate change will influence food webs and nutrient dynamics.

The projected mid-century reductions in oyster growth obtained from this analysis are consistent with the results of other studies that examine oyster growth under similar projected climate change conditions. A study modeling oyster responses to warming and low salinity co-stressors in Barataria Bay, LA, for example, predicts that under a warming and high flow scenario (though without the effects of future nutrient reductions or atmospheric CO_2), oysters will experience widespread mortality in fresher parts of the bay by the end of the century (Lavaud et al., 2021). Experimental studies have shown similar negative effects of acidification, warming, lower food availability, and increased freshwater flow on oyster survival (La Peyre et al., 2013; Rybovich et al., 2016; Lowe et al., 2019; Jones et al., 2019). Da (2023) found that the reductions in salinity and Ω_{Ca} that result from high discharge events in the York River will increase in extent as climate change progresses and increasingly threaten aquaculture production. In the Chesapeake Bay, extreme precipitation events are predicted to occur more frequently with future climate change, however an overall decline in annual average precipitation is also predicted (St. Laurent et al., 2021). As a result, the overall impact of freshwater from the land is not projected to change significantly in the future (Hinson et al., 2023). Changes in precipitation were thus not simulated in this study, but future work could examine the dynamics of climate change, salinity, Ω_{Ca}, and oyster growth in a year with more heavy rainfall events but lower annual rainfall.

4.3 Influence of future changes in oyster growth on aquaculture

Understanding the relative impacts of global climate change and local nutrient management actions on oyster growth and survival will allow aquaculture producers to anticipate how their oyster stock may respond to these anthropogenic changes. As the effects of climate change are subject to natural interannual variability, the magnitude of acidification and warming in a given year will likely differ (Cai et al., 2021; Moore-Maley et al., 2016; Li et al., 2016), influencing oyster growth through differing mechanisms. Smaller oysters resulting from slower growing times in a particularly warm year may present a different challenge to growers than weak-shelled oysters in a year with lower Ω_{Ca} and average temperatures. Mortality may also become a more urgent challenge as summer temperatures warm. A previous study examining commercial performance of Pacific oysters in Brazil found that interannual variability in temperature, chl*a* abundance, and climate events influenced survival and growth phase timing (Mizuta et al., 2012). High temperatures inhibited survival of oyster seed in that study, which frequently occurs in Pacific oysters (*Crassostrea gigas)* during the summer months in Europe and California (Goulletquer et al., 1998; Burge et al., 2007; Malhan et al., 2009). A similar phenomenon has been observed in Eastern oysters; however, mortality events in this species have not been conclusively linked to warmer water temperatures (Guevelou et al., 2019; Biranik and Allam, 2023), and the cause is yet to be resolved for either species and remains an area of active research. Nonetheless, the increasing occurrence of spring/summer mortality in Eastern oysters suggests that shifting the time of planting oysters on

553   leases later in the year may help mitigate the risk of widespread mortality, although the economic tradeoffs involved in shifting

554   the growing season for oysters should be taken into account.

555   Future climate change and nutrient management are projected to worsen conditions for oyster growth, and the spatial

556   variation in these changes may unevenly influence aquaculture production. While reductions in shell and tissue growth are

557   predicted for nearly all regions where oysters grow, these changes will likely differ based on present-day environmental

558   conditions. Under present day conditions, the most oyster growth is projected to occur in regions with some of the highest

559   present-day Ω_{Ca} and the greatest projected Ω_{Ca} reductions, i.e., in the Rappahannock River and mainstem shoals. Some of the

560   most dramatic tissue and shell reductions are projected to occur in the York and upper Rappahannock, where reduced food

561   availability and low Ω_{Ca} will limit oyster filtration and shell growth. Oysters in parts of both the Rappahannock and York

562   Rivers will likely face mortality (represented by near complete depletion of oyster shell and tissue) by mid-century (Figs. 8,

563   9). However, these reductions will not be spatially uniform, underscoring the importance of oyster farm site selection within a

564   tributary. In contrast, oysters grown outside the tributaries are projected to exhibit a smaller decline in growth, indicating

565   greater future opportunity for oyster farming in these locations. Under the business-as-usual climate change trajectory analyzed

566   here, bottom conditions in the tributaries will be less suitable for oyster aquaculture by mid-century, and producers might

567   consider alternate farm locations or shifting production methods toward floating culture to avoid exposure to low Ω_{Ca}

568   conditions and access greater food availability.

569   Beyond reduced oyster growth, aquaculture operations may also be affected in the future by temporal changes in

570   optimal growing conditions. Due to the input of freshwater that lowers DIC and TA and increases pCO$_2$ (Cai et al., 2017; Cai

571   et al., 2021; Da et al., 2024), the greatest magnitude of Ω_{Ca} reductions occurs in spring. The majority of oyster growth is

572   projected to occur in the spring and summer (Fig. 5), so changes to growing conditions may be most consequential during

573   these warmer months. Deployment of oyster seed generally begins in the spring and continues into the summer, so it is

574   important for producers to be aware of ambient conditions being experienced by their newly deployed oysters. As spring

575   temperatures warm, phytoplankton blooms will likely occur earlier in the year, shifting the time when food availability is

576   highest (Da et al., 2021). Oysters deployed earlier in the year may benefit from greater food availability and perform better

577   than oysters deployed in July or August when waters are warmest. However, they may also face the challenge of spring/summer

578   mortality events, revealing the complexity of timing oyster deployment under worsening climate change conditions. For oyster

579   farms closer to freshwater sources, the combined effects of low Ω_{Ca}, low salinity, and high summer temperatures may severely

580   inhibit growth and extend time-to-market. This study focused on diploid oysters, since the laboratory experiments used to

581   develop the EcoOyster model parameterizations were conducted on diploids. Future laboratory experiments with triploids

582   would enhance our modeling efforts for triploid oysters, which are commonly used in aquaculture in the Chesapeake Bay

583   region.

4.4 Future work

Providing the aquaculture industry with the best existing estimates of climate change impacts to their operations will allow them to make more informed decisions about their future practices. This study used a 120-meter horizontal resolution model grid to examine near-lease-level effects of climate change and management actions on oyster growth in a section of the lower Chesapeake Bay. Similar studies with high resolution model grids in other systems will strengthen our understanding of how regional anthropogenic effects will influence the oyster aquaculture sector and could be used to identify areas of opportunity for new aquaculture practices (Swam et al., 2022; Palmer et al., 2021; Lavaud et al., 2024). The present study incorporated one Earth System Model and one emissions scenario; future work should quantify how these choices impact estimates of future Ω_{Ca} and oyster growth (e.g., Hinson et al., 2023). Future modeling studies should also incorporate other climate change impacts, such as sea level rise and increased storminess which are projected to influence conditions for oyster growth in the Chesapeake Bay region (Seneviratne et al., 2012; Lowe et al., 2019, Rybovich et al., 2016, Jones et al., 2019).

To improve estimates of shell and tissue growth of oysters under climate change, additional experimental studies should be conducted to reduce the data gaps that currently limit model formulations. Uncertainties in the functional relationships and rate parameters used in these models may lead to an inaccurate influence of some environmental variables on oyster growth. For example, results in this study may be particularly sensitive to the optimum temperature for filtration rate. Reductions in tissue weight are particularly dramatic when average temperature conditions at oyster lease sites remain above this optimal temperature from mid-June through late August, a vital time for oyster growth. Many physiological studies of temperature impacts on oyster filtration date back to the mid-to-late-20th century, and present-day seasonal extremes that coastal organisms experience may routinely exceed the maximum temperatures used in many of these earlier experimental designs. For example, Jordan (1987) used a maximum temperature of 27 °C, which was the ambient temperature when samples were collected in July from the Choptank River, MD. Between 1985 and 2014, bottom waters of the north mesohaline Bay main stem (closest to the Choptank) warmed 1.01 ± 0.13 °C during May to October (Hinson et al., 2022), and the present study predicts a 1.5 ± 0.26 °C increase across the entire model domain between 2017 and mid-century. To build stronger models of future climate impacts, and to expand scientific understanding of physiological limits of the Eastern oyster, future studies should re-examine temperature limitations on oyster filtration and respiration by using higher experimental temperatures.

As oyster growth is highly sensitive to food availability, improved measurements of particulate organic carbon in the region would fortify projections of oyster production under future climate change and nutrient management. Here, it is assumed that oysters feed on POC, a combination of plankton and detritus. However, average POC concentrations are highly spatiotemporally variable in the Chesapeake Bay due to eutrophication and algal blooms. In this study, POC was underestimated in the tributary channels; however, it is unclear how well POC was estimated in oyster growing areas, as *in situ* measurements are currently limited to stations in the channels during monthly or semi-monthly sampling cruises. More routine POC measurements, as well as measurements of POC in regions where oyster farming operations occur, are needed to

616 verify the spatiotemporal dynamics of food availability. Improved measurements of oyster food availability would allow for

617 stronger model skill assessment and improved projections of oyster production.

618 **5 Conclusions**

619   This study predicts widespread reductions in Ω_{Ca} in the lower Virginia tributaries of the Chesapeake Bay by mid-

620 century, highlighting the use of high-resolution model projections to better understand present-day carbonate chemistry

621 conditions and to predict the effects of climate change on a region of high interest for aquaculture production. While similar

622 modeling studies have projected acidification conditions in coastal regions with 3D coupled models (Siedlecki et al., 2021a,b;

623 Fujii et al., 2023) or modeled oyster growth with remote-sensing data and dynamic energy budget models (Palmer et al., 2020;

624 Palmer et al., 2021; Bertollini et al., 2021), the present study projects both carbonate chemistry conditions and oyster

625 bioenergetics in the Chesapeake Bay with the highest resolution thus far. Specifically, widespread reductions in Ω_{Ca} will

626 negatively impact oyster growth, with implications for aquaculture operations and local and regional economies. As bottom

627 conditions worsen, altered site-selection for oyster farms or other adaptive measures will become imperative to sustain

628 production and reduce the impacts of low Ω_{Ca} on farmed oysters.

629   Increased atmospheric CO_2 and nutrient reductions are projected to inhibit oyster calcification, while warming and

630 nutrient reductions will reduce oyster tissue and shell growth due to limitations on filtration and lowered food availability.

631 While the effects of global climate change on oyster growth are projected to be much stronger overall than the effects of local

632 nutrient management, lowered food availability from nutrient reductions may have a strong influence on oyster growth in

633 certain parts of the study region. As a result, all areas will not be equally vulnerable to future changes in the atmosphere and

634 watershed. Understanding how individual drivers influence oyster growth is important for predicting effects on aquaculture

635 production in the context of interannual variability of climate change and nutrient management outcomes. While the negative

636 effects of temperature on growth were strong in this study, additional studies on Eastern oyster temperature limits are needed

637 to improve projections, particularly as summer mortality of oysters is already common. Increased *in situ* measurements of

638 biogeochemical variables and experimental studies on oyster physiology and bioenergetics will allow for improved projections

639 of mid-century conditions and their potential impacts on oyster growth and the aquaculture industry.

640

641 **Code Availability**

642 Model code will be available upon request.

643

644 **Data Availability**

645 Model output will be available with a DOI on William & Mary ScholarWorks.

646

647 **Author Contribution**

648 MAMF, EBR, MJB, and PS wrote the proposal and acquired the funding for the project; MAMF, PS, and FD developed the
649 ROMS-ECB code; MJB developed the EcoOyster code; CC, MAMF, and EBR designed the experiment; CC ran model
650 simulations, analyzed the output, created the figures, and wrote the manuscript draft; MAMF, EBR, MJB, PS, and FD reviewed
651 and edited the manuscript.
652

653 **Competing Interests**
654 The authors declare that they have no conflict of interest.
655

656 **Acknowledgements**
657 This paper is the result of research funded by the National Oceanic and Atmospheric Administration's Ocean Acidification
658 Program under award NA18OAR0170430 to the Virginia Institute of Marine Science (VIMS). We would like to thank the
659 VIMS and William & Mary (W&M) high performance computing group for their technical support and computing resources.
660 We also thank the NOAA Chesapeake Bay Program for providing us with watershed inputs from their Phase 6 Watershed
661 Model. This work was largely made possible by Sara Blachman's hard work on the EcoOyster model. We thank Bill Walton
662 for his aquaculture expertise and support throughout the project. The model results used for this manuscript are available at
663 W&M Scholarworks.

664 **References**

665 Abatzoglou, J. T. and Brown, T. J.: A comparison of statistical downscaling methods suited for wildfire applications, Int. J.
666 Clim., 32, 772–780, https://doi.org/10.1002/joc.2312, 2012.
667 Allen, K. L., Ihde, T., Knoche, S., Townsend, H., & Lewis, K. A.: Simulated climate change impacts on striped bass, blue crab
668 and Eastern oyster in oyster sanctuary habitats of Chesapeake Bay. Estuar. Coast. Shelf Sci., 292, 108465,
669 https://doi.org/10.1016/j.ecss.2023.108465, 2023.
670 Amaral, V., Cabral, H. N., and Bishop, M. J.: Effects of estuarine acidification on predator–prey interactions. Mar. Eco. Prog.
671 Ser., 445, 117-127, https://doi.org/10.3354/meps09487, 2012.
672 Barclay, K.M., Gingras, M.K., Packer, S.T. and Leighton, L.R.: The role of gastropod shell composition and microstructure in
673 resisting dissolution caused by ocean acidification, Mar. Environ. Res., 162, 105105,
674 https://doi.org/10.1016/j.marenvres.2020.105105, 2020.
675 Barton, S. and Yvon-Durocher, G.: Quantifying the temperature dependence of growth rate in marine phytoplankton within
676 and across species, Limnol. Oceanogr., 64, 2081–2091, https://doi.org/10.1002/lno.11170, 2019.
677 Beniash, E., Ivanina, A., Lieb, N., Kurochkin, I., and Sokolova, I.: Elevated level of carbon dioxide affects metabolism and
678 shell formation in oysters Crassostrea virginica (Gmelin), Mar. Ecol. Prog. Ser., 419, 95–108,
679 https://doi.org/10.3354/meps08841, 2010.

680 Bertolini, C., Brigolin, D., Porporato, E. M. D., Hattab, J., Pastres, R., and Tiscar, P. G.: Testing a Model of Pacific Oysters'
681 (Crassostrea gigas) Growth in the Adriatic Sea: Implications for Aquaculture Spatial Planning, Sustainability, 13, 3309,
682 https://doi.org/10.3390/su13063309, 2021.

683 Bhatt, G., Linker, L., Shenk, G., Bertani, I., Tian, R., Rigelman, J., Hinson, K., and Claggett, P.: Water quality impacts of
684 climate change, land use, and population growth in the Chesapeake Bay watershed, JAWRA J. Am. Water Resour. Assoc., 59,
685 1313–1341, https://doi.org/10.1111/1752-1688.13144, 2023.

686 Borges, A. V. and Gypens, N.: Carbonate chemistry in the coastal zone responds more strongly to eutrophication than to ocean
687 acidification, Limnol. Oceanogr., 55, 346–353, https://doi.org/10.4319/lo.2010.55.1.0346, 2010.

688 Boulais, M., Chenevert, K. J., Demey, A. T., Darrow, E. S., Robison, M. R., Roberts, J. P., and Volety, A.: Oyster reproduction
689 is compromised by acidification experienced seasonally in coastal regions, Sci. Rep., 7, 13276, https://doi.org/10.1038/s41598-
690 017-13480-3, 2017.

691 Brianik, C. J. and Allam, B.: The need for more information on the resistance to biological and environmental stressors in
692 triploid oysters, Aquaculture, 577, 739913, https://doi.org/10.1016/j.aquaculture.2023.739913, 2023.

693 Bukaveckas, P. A.: Carbon dynamics at the river–estuarine transition: a comparison among tributaries of Chesapeake Bay,
694 Biogeosciences, 19, 4209–4226, https://doi.org/10.5194/bg-19-4209-2022, 2022.

695 Brush, M.J., and M.L. Kellogg: Harris Creek Oyster Restoration Model v2. Virginia Institute of Marine Science, Gloucester
696 Point, VA, https://www.vims.edu/research/departments/bio/programs/semp/models/index.php, 2018.

697 Burford, M., Scarpa, J., Cook, B., and Hare, M.: Local adaptation of a marine invertebrate with a high dispersal potential:
698 evidence from a reciprocal transplant experiment of the eastern oyster Crassostrea virginica, Mar. Ecol. Prog. Ser., 505, 161–
699 175, https://doi.org/10.3354/meps10796, 2014.

700 Burge, C. A., Judah, L. R., Conquest, L. L., Griffin, F. J., Cheney, D. P., Suhrbier, A., Vadopalas, B., Olin, P. G., Renault, T.,
701 and Friedman, C. S.: Summer seed mortality of the pacific oyster, Crassostrea gigas (Thunberg) grown in Tomales Bay,
702 California, USA: the influence of oyster stock, planting time, pathogens, and environmental stressors, J. Shellfish Res,
703 https://doi.org/10.2983/0730-8000, 2007.

704 Cai, W., Feely, R. A., Testa, J. M., Li, M., Evans, W., Alin, S. R., Xu, Y.-Y., Pelletier, G., Ahmed, A., Greeley, D. J., Newton,
705 J. A., and Bednaršek, N.: Natural and Anthropogenic Drivers of Acidification in Large Estuaries, Annu. Rev. Mar. Sci.,
706 https://doi.org/10.1146/annurev-marine-010419-011004, 2021.

707 Cai, W.J., Huang, W.-J., Luther, G. W., Pierrot, D., Li, M., Testa, J., Xue, M., Joesoef, A., Mann, R., Brodeur, J., Xu, Y.-Y.,
708 Chen, B., Hussain, N., Waldbusser, G. G., Cornwell, J., and Kemp, W. M.: Redox reactions and weak buffering capacity lead
709 to acidification in the Chesapeake Bay, Nat. Commun., 8, 369, https://doi.org/10.1038/s41467-017-00417-7, 2017.

710 Cai, W.J., Xu, Y.-Y., Feely, R. A., Wanninkhof, R., Jönsson, B., Alin, S. R., Barbero, L., Cross, J. N., Azetsu-Scott, K.,
711 Fassbender, A. J., Carter, B. R., Jiang, L.-Q., Pepin, P., Chen, B., Hussain, N., Reimer, J. J., Xue, L., Salisbury, J. E.,
712 Hernández-Ayón, J. M., Langdon, C., Li, Q., Sutton, A. J., Chen, C.-T. A., and Gledhill, D. K.: Controls on surface water

713   carbonate chemistry along North American ocean margins, Nat. Commun., 11, 2691, https://doi.org/10.1038/s41467-020-
714   16530-z, 2020.

715   Cai, W. J., and Wang, Y.: The chemistry, fluxes, and sources of carbon dioxide in the estuarine waters of the Satilla and
716   Altamaha Rivers, Georgia. Limnol. Oceanogr., 43(4), 657-668, https://doi.org/10.4319/lo.1998.43.4.0657, 1998.

717   Caldeira, K. and Wickett, M. E.: Anthropogenic carbon and ocean pH, Nature, 425, 365–365, https://doi.org/10.1038/425365a,
718   2003.

719   Caillon, C., Fleury, E., Di Poi, C., Gazeau, F., and Pernet, F.: Food availability, but not tidal emersion, influences the combined
720   effects of ocean acidification and warming on oyster physiological performance, Aquaculture, 742459,
721   https://doi.org/10.1016/j.aquaculture.2025.742459, 2025.

722   Caldeira, K. and Wickett, M. E.: Ocean model predictions of chemistry changes from carbon dioxide emissions to the
723   atmosphere and ocean, J. Geophys. Res.: Oceans, 110, https://doi.org/10.1029/2004jc002671, 2005.

724   Callam, B. R., Allen, S. K., and Frank-Lawale, A.: Genetic and environmental influence on triploid Crassostrea virginica
725   grown in Chesapeake Bay: Growth, Aquaculture, 452, 97–106, https://doi.org/10.1016/j.aquaculture.2015.10.027, 2016.

726   Carstensen, J. and Duarte, C. M.: Drivers of pH Variability in Coastal Ecosystems, Environ. Sci. Technol., 53, 4020–4029,
727   https://doi.org/10.1021/acs.est.8b03655, 2019.

728   Cerco, C. and Noel, M.: Process-based primary production modeling in Chesapeake Bay, Mar. Ecol. Prog. Ser., 282, 45–58,
729   https://doi.org/10.3354/meps282045, 2004.

730   Cerco, C. F. and Noel, M. R.: Nonnative Oysters in the Chesapeake Bay, 2005.

731   Cerco, C. F., Noel, M. R., and Wang, P.: The Shallow-Water Component of the Chesapeake Bay Environmental Model
732   Package, JAWRA J. Am. Water Resour. Assoc., 49, 1091–1102, https://doi.org/10.1111/jawr.12106, 2013.

733   Chesapeake Bay Program DataHub: https://datahub.chesapeakebay.net/, last access: 28 January 2024

734   Comeau, L. A., Mayrand, É., and Mallet, A.: Winter quiescence and spring awakening of the Eastern oyster Crassostrea
735   virginica at its northernmost distribution limit, Mar. Biol., 159, 2269–2279, https://doi.org/10.1007/s00227-012-2012-8, 2012.

736   Copernicus Climate Change Service: ERA5: Fifth Generation of ECMWF Atmospheric Reanalyses of the Global Climate,
737   Copernicus Climate Change Service Climate Data Store (CDS). https://cds.climate.copernicus.eu/cdsapp#!/home, 2017.

738   Da, F., Friedrichs, M. A. M., St-Laurent, P., Shadwick, E. H., Najjar, R. G., and Hinson, K. E.: Mechanisms Driving Decadal
739   Changes in the Carbonate System of a Coastal Plain Estuary, J. Geophys. Res.: Oceans, 126,
740   https://doi.org/10.1029/2021jc017239, 2021.

741   Da, F: Chesapeake Bay Carbon Cycle: Past, Present, Future, PhD. Dissertation, Virginia Institute of Marine Science, William
742   & Mary, Virginia, USA, https://dx.doi.org/10.25773/v5-46f7-e286, 2023.

743   Da, F., Friedrichs, M. A. M., St-Laurent, P., Najjar, R. G., Shadwick, E. H., and Stets, E. G.: Influence of Rivers, Tides, and
744   Tidal Wetlands on Estuarine Carbonate System Dynamics, Estuaries Coasts, 1-23, https://doi.org/10.1007/s12237-024-01421-
745   z, 2024.

746 Dame, R.F.: The ecological energies of growth, respiration and assimilation in the intertidal American oyster Crassostrea

747 virginica, Mar. Biol., 17, 43-250, 1972.

748 Dayton, P.K.: Toward an understanding of community resilience and the potential effects of enrichments to the benthos at

749 McMurdo Sound, Antarctica, Proceedings of the colloquium on conservation problems in Antarctica, 81-96, 1972.

750 Dégremont, L., Garcia, C., Frank-Lawale, A., and Allen, S. K.: Triploid Oysters in the Chesapeake Bay: Comparison of Diploid

751 and Triploid Crassostrea virginica, J. Shellfish Res., 31, 21–31, https://doi.org/10.2983/035.031.0103, 2012.

752 Dickinson, G. H., Ivanina, A. V., Matoo, O. B., Pörtner, H. O., Lannig, G., Bock, C., Beniash, E., and Sokolova, I. M.:

753 Interactive effects of salinity and elevated CO_2 levels on juvenile eastern oysters, Crassostrea virginica, J. Exp. Biol., 215, 29–

754 43, https://doi.org/10.1242/jeb.061481, 2011.

755 Dinauer, A. and Mucci, A.: Spatial variability in surface-water pCO 2 and gas exchange in the world's largest semi-enclosed

756 estuarine system: St. Lawrence Estuary (Canada), Biogeosciences, 14, 3221-3237, https://doi.org/10.5194/bg-14-3221-2017,

757 2017.

758 Doney, S. C., Fabry, V. J., Feely, R. A., and Kleypas, J. A.: Ocean acidification: the other CO_2 problem., Annu. Rev. Mar.

759 Sci., 1, 169–92, https://doi.org/10.1146/annurev.marine.010908.163834, 2009.

760 Dong, S., Lei, Y., Li, T., Cao, Y., and Xu, K.: Biocalcification crisis in the continental shelf under ocean acidification. Geosci.

761 Front., 14(6), 101622, https://doi.org/10.1016/j.gsf.2023.101622, 2023.

762 Du, J., Shen, J., Park, K., Wang, Y. P., and Yu, X.: Worsened physical condition due to climate change contributes to the

763 increasing hypoxia in Chesapeake Bay, Sci. Total Environ., 630, 707–717, https://doi.org/10.1016/j.scitotenv.2018.02.265,

764 2018.

765 Duarte, C. M., Hendriks, I. E., Moore, T. S., Olsen, Y. S., Steckbauer, A., Ramajo, L., Carstensen, J., Trotter, J. A., and

766 McCulloch, M.: Is Ocean Acidification an Open-Ocean Syndrome? Understanding Anthropogenic Impacts on Seawater pH,

767 Estuaries Coasts, 36, 221–236, https://doi.org/10.1007/s12237-013-9594-3, 2013.

768 Dufresne, J.-L., Foujols, M.-A., Denvil, S., Caubel, A., Marti, O., Aumont, O., Balkanski, Y., Bekki, S., Bellenger, H.,

769 Benshila, R., Bony, S., Bopp, L., Braconnot, P., Brockmann, P., Cadule, P., Cheruy, F., Codron, F., Cozic, A., Cugnet, D.,

770 Noblet, N. de, Duvel, J.-P., Ethé, C., Fairhead, L., Fichefet, T., Flavoni, S., Friedlingstein, P., Grandpeix, J.-Y., Guez, L.,

771 Guilyardi, E., Hauglustaine, D., Hourdin, F., Idelkadi, A., Ghattas, J., Joussaume, S., Kageyama, M., Krinner, G., Labetoulle,

772 S., Lahellec, A., Lefebvre, M.-P., Lefevre, F., Levy, C., Li, Z. X., Lloyd, J., Lott, F., Madec, G., Mancip, M., Marchand, M.,

773 Masson, S., Meurdesoif, Y., Mignot, J., Musat, I., Parouty, S., Polcher, J., Rio, C., Schulz, M., Swingedouw, D., Szopa, S.,

774 Talandier, C., Terray, P., Viovy, N., and Vuichard, N.: Climate change projections using the IPSL-CM5 Earth System Model:

775 from CMIP3 to CMIP5, Clim. Dyn., 40, 2123–2165, https://doi.org/10.1007/s00382-012-1636-1, 2013.

776 Dunne, J. P., John, J. G., Adcroft, A. J., Griffies, S. M., Hallberg, R. W., Shevliakova, E., Stouffer, R. J., Cooke, W., Dunne,

777 K. A., Harrison, M. J., Krasting, J. P., Malyshev, S. L., Milly, P. C. D., Phillipps, P. J., Sentman, L. T., Samuels, B. L., Spelman,

778 M. J., Winton, M., Wittenberg, A. T., and Zadeh, N.: GFDL's ESM2 Global Coupled Climate–Carbon Earth System Models.

Part I: Physical Formulation and Baseline Simulation Characteristics, J. Clim., 25, 6646–6665, https://doi.org/10.1175/jcli-d-11-00560.1, 2012.

EPA, Chesapeake Bay Total Maximum Daily Load for Nitrogen, Phosphorus, and Sediment, United States Environmental Protection Agency, 2010.

Guinotte, J. M. and Fabry, V. J.: Ocean Acidification and Its Potential Effects on Marine Ecosystems, Ann. N. York Acad. Sci., 1134, 320–342, https://doi.org/10.1196/annals.1439.013, 2008.

Ehrich, M. K. and Harris, L. A.: A review of existing eastern oyster filtration rate models, Ecol. Model., 297, 201–212, https://doi.org/10.1016/j.ecolmodel.2014.11.023, 2015.

Feely, R. A., Sabine, C. L., Lee, K., Berelson, W., Kleypas, J., Fabry, V. J., and Millero, F. J.: Impact of Anthropogenic CO_2 on the $CaCO_3$ System in the Oceans, Science, 305, 362–366, https://doi.org/10.1126/science.1097329, 2004.

Feely, R. A., Doney, S. C., and Cooley, S. R.: Ocean Acidification: Present Conditions and Future Changes in a High-CO_2 World, Oceanography, 22, 36–47, https://doi.org/10.5670/oceanog.2009.95, 2009.

Feng, Y., Friedrichs, M. A. M., Wilkin, J., Tian, H., Yang, Q., Hofmann, E. E., Wiggert, J. D., and Hood, R. R.: Chesapeake Bay nitrogen fluxes derived from a land-estuarine ocean biogeochemical modeling system: Model description, evaluation, and nitrogen budgets, J. Geophys. Res.: Biogeosciences, 120, 1666–1695, https://doi.org/10.1002/2015jg002931, 2015.

Fitzer, S. C., Torres Gabarda, S., Daly, L., Hughes, B., Dove, M., O'Connor, W., Potts, J., Scanes, P., and Byrne, M.: Coastal acidification impacts on shell mineral structure of bivalve mollusks. Ecol. Evol., 8(17), 8973-8984, https://doi.org/10.1002/ece3.4416, 2018.

Frankel, L. T., Friedrichs, M. A. M., St-Laurent, P., Bever, A. J., Lipcius, R. N., Bhatt, G., and Shenk, G. W.: Nitrogen reductions have decreased hypoxia in the Chesapeake Bay: Evidence from empirical and numerical modeling, Sci. Total Environ., 814, 152722, https://doi.org/10.1016/j.scitotenv.2021.152722, 2022.

Frank-Lawale, A., Allen, S. K., and Dgremont, L.: Breeding and Domestication of Eastern Oyster (Crassostrea virginica) Lines for Culture in the Mid-Atlantic, Usa: Line Development and Mass Selection for Disease Resistance, J. Shellfish Res., 33, 153–165, https://doi.org/10.2983/035.033.0115, 2014.

Fujii, M., Hamanoue, R., Bernardo, L. P. C., Ono, T., Dazai, A., Oomoto, S., Wakita, M., and Tanaka, T.: Assessing impacts of coastal warming, acidification, and deoxygenation on Pacific oyster (Crassostrea gigas) farming: a case study in the Hinase area, Okayama Prefecture, and Shizugawa Bay, Miyagi Prefecture, Japan, Biogeosciences, 20, 4527–4549, https://doi.org/10.5194/bg-20-4527-2023, 2023.

Fulford, R., Breitburg, D., Newell, R., Kemp, W., and Luckenbach, M.: Effects of oyster population restoration strategies on phytoplankton biomass in Chesapeake Bay: a flexible modeling approach, Mar. Ecol. Prog. Ser., 336, 43–61, https://doi.org/10.3354/meps336043, 2007.

Gattuso, Strong, A. L., Kroeker, K. J., Teneva, L. T., Mease, L. A., and Kelly, R. P.: Ocean Acidification 2.0: Managing our Changing Coastal Ocean Chemistry, BioScience, 64, 581–592, https://doi.org/10.1093/biosci/biu072, 2014.

812 Gawde, R. K., North, E. W., Hood, R. R., Long, W., Wang, H., and Wilberg, M. J.: A high resolution hydrodynamic-
813 biogeochemical-oyster-filtration model predicts that the presence of oysters (Crassostrea virginica) can improve, or reduce,
814 water quality depending upon oyster abundance and location. Ecol. Model., 496, 110833,
815 https://doi.org/10.1016/j.ecolmodel.2024.110833, 2024.

816 Gazeau, F., Quiblier, C., Jansen, J. M., Gattuso, J. P., Middelburg, J. J., and Heip, C. H.: Impact of elevated CO_2 on shellfish
817 calcification. Geophys. Res. Lett., 34, 7, https://doi.org/10.1029/2006GL028554, 2007.

818 Gobler, C. J. and Talmage, S. C.: Physiological response and resilience of early life-stage Eastern oysters (Crassostrea
819 virginica) to past, present and future ocean acidification, Conserv. Physiol., 2, cou004,
820 https://doi.org/10.1093/conphys/cou004, 2014.

821 Goulletquer, P., Soletchnik, P., Le Moine, O., Razet, D., Geairon, P., and Faury, N.: Summer mortality of the Pacific cupped
822 oyster Crassostrea gigas in the Bay of Marennes-Oléron (France), CIEM Conseil International pour l'Exploration de la Mer,
823 1998.

824 Gmelin, J. F.: Caroli a Linnaei Systema Naturae per Regna Tria Naturae, *Systema Naturae, Linneaeus, 13,* 3021-3910, 1791.

825 Gruber, N., Clement, D., Carter, B. R., Feely, R. A., Heuven, S. van, Hoppema, M., Ishii, M., Key, R. M., Kozyr, A., Lauvset,
826 S. K., Monaco, C. L., Mathis, J. T., Murata, A., Olsen, A., Perez, F. F., Sabine, C. L., Tanhua, T., and Wanninkhof, R.: The
827 oceanic sink for anthropogenic CO_2 from 1994 to 2007, Science, 363, 1193–1199, https://doi.org/10.1126/science.aau5153,
828 2019.

829 Guévélou, E., Carnegie, R. B., Small, J. M., Hudso n, K., Reece, K. S., and Rybovich, M. M.: Tracking Triploid Mortalities
830 of Eastern Oysters Crassostrea virginica in the Virginia Portion of the Chesapeake Bay, J. Shellfish Res., 38, 101–113,
831 https://doi.org/10.2983/035.038.0110, 2019.

832 Hasler, C. T., Jeffrey, J. D., Schneider, E. V. C., Hannan, K. D., Tix, J. A., and Suski, C. D.: Biological consequences of weak
833 acidification caused by elevated carbon dioxide in freshwater ecosystems, Hydrobiologia, 806, 1–12,
834 https://doi.org/10.1007/s10750-017-3332-y, 2018.

835 Herrmann, M., Najjar, R. G., Da, F., Friedman, J. R., Friedrichs, M. A. M., Goldberger, S., Menendez, A., Shadwick, E. H.,
836 Stets, E. G., and St-Laurent, P.: Challenges in Quantifying Air-Water Carbon Dioxide Flux Using Estuarine Water Quality
837 Data: Case Study for Chesapeake Bay, J. Geophys. Res.: Oceans, 125, e2019JC015610, https://doi.org/10.1029/2019jc015610,
838 2020.

839 Hersbach, H., Bell, B., Berrisford, P., Hirahara, S., Horányi, A., Muñoz-Sabater, J., Nicolas, J., Peubey, C., Radu, R., Schepers,
840 D., Simmons, A., Soci, C., Abdalla, S., Abellan, X., Balsamo, G., Bechtold, P., Biavati, G., Bidlot, J., Bonavita, M., Chiara,
841 G., Dahlgren, P., Dee, D., Diamantakis, M., Dragani, R., Flemming, J., Forbes, R., Fuentes, M., Geer, A., Haimberger, L.,
842 Healy, S., Hogan, R. J., Hólm, E., Janisková, M., Keeley, S., Laloyaux, P., Lopez, P., Lupu, C., Radnoti, G., Rosnay, P.,
843 Rozum, I., Vamborg, F., Villaume, S., and Thépaut, J.: The ERA5 global reanalysis, Q. J. R. Meteorol. Soc., 146, 1999–2049,
844 https://doi.org/10.1002/qj.3803, 2020.

Hinson, K. E., Friedrichs, M. A. M., St-Laurent, P., Da, F., and Najjar, R. G.: Extent and Causes of Chesapeake Bay Warming, JAWRA J. Am. Water Resour. Assoc., 58, 805–825, https://doi.org/10.1111/1752-1688.12916, 2022.

Hinson, K. E., Friedrichs, M. A. M., Najjar, R. G., Herrmann, M., Bian, Z., Bhatt, G., St-Laurent, P., Tian, H., and Shenk, G.: Impacts and uncertainties of climate-induced changes in watershed inputs on estuarine hypoxia, Biogeosciences, 20, 1937–1961, https://doi.org/10.5194/bg-20-1937-2023, 2023.

Hinson, K.E., Friedrichs, M. A. M., Najjar, R. G., Bian, Z., Herrmann, M., St-Laurent, P., 2024. Response of hypoxia to future climate change is sensitive to methodological assumptions. Scientific Reports, 14, 17544, https://doi.org/10.1038/s41598-024-68329-3

Himes, A.R., Schatz, A. and Rivest, E.B.: Differences in larval acidification tolerance among populations of the eastern oyster, Crassostrea virginica. J. Exp. Mar. Biol. Ecol., 577, 152023, https://doi.org/10.1016/j.jembe.2024.152023, 2024.

Hochachka, P. W. and Somero, G. N.: Biochemical Adaptation: Mechanism and Processing Physiological Evolution. Oxford University Press, 2002.

Hofmann, G. E. and Hand, S. C.: Global arrest of translation during invertebrate quiescence., Proc. Natl. Acad. Sci., 91, 8492–8496, https://doi.org/10.1073/pnas.91.18.8492, 1994.

Hopkinson, C. S., Buffam, I., Hobbie, J., Vallino, J., Perdue, M., Eversmeyer, B., Prahl, F., Covert, J., Hodson, R., Moran, M. A., Smith, E., Baross, J., Crump, B., Findlay, S., and Foreman, K.: Terrestrial inputs of organic matter to coastal ecosystems: An intercomparison of chemical characteristics and bioavailability, Biogeochemistry, 43, 211–234, https://doi.org/10.1023/a:1006016030299, 1998.

Hudson, K.: Virginia Shellfish Aquaculture Situation and Outlook Report:Results of the 2018 Virginia Shellfish Aquaculture Crop Reporting Survey, 2019.

Intergovernmental Panel on Climate Change: IPCC Special Report on the Ocean and Cryosphere in a Changing Climate [H.-O. Pörtner, D.C. Roberts, V. Masson-Delmotte, P. Zhai, M. Tignor, E. Poloczanska, K. Mintenbeck, A. Alegría, M. Nicolai, A. Okem, J. Petzold, B. Rama, N.M. Weyer (eds.)]. Cambridge University Press, Cambridge, UK and New York, NY, USA, 755 pp. https://doi.org/10.1017/9781009157964, 2019.

Intergovernmental Panel on Climate Change: The Physical Science Basis, 673–816, https://doi.org/10.1017/9781009157896.007, 2021.

Irby, I. D., Friedrichs, M. A. M., Friedrichs, C. T., Bever, A. J., Hood, R. R., Lanerolle, L. W. J., Li, M., Linker, L., Scully, M. E., Sellner, K., Shen, J., Testa, J., Wang, H., Wang, P., and Xia, M.: Challenges associated with modeling low-oxygen waters in Chesapeake Bay: a multiple model comparison, Biogeosciences, 13, 2011–2028, https://doi.org/10.5194/bg-13-2011-2016, 2016.

Irby, I. D., Friedrichs, M. A. M., Da, F., and Hinson, K. E.: The competing impacts of climate change and nutrient reductions on dissolved oxygen in Chesapeake Bay, Biogeosciences, 15, 2649–2668, https://doi.org/10.5194/bg-15-2649-2018, 2018.

Jewett, L. and Romanou, A: Ocean acidification and other ocean changes. In: Climate Science Special Report: Fourth National Climate Assessment, Volume I [Wuebbles, D.J., D.W. Fahey, K.A. Hibbard, D.J. Dokken, B.C. Stewart, and T.K. Maycock (eds.)]. U.S. Global Change Research Program, Washington, DC, USA, pp. 364-392, doi: 10.7930/J0QV3JQB, 2017.

Jones, H. R., Johnson, K. M., and Kelly, M. W.: Synergistic Effects of Temperature and Salinity on the Gene Expression and Physiology of Crassostrea virginica, Integr. Comp. Biol., 59, 306–319, https://doi.org/10.1093/icb/icz035, 2019.

Jordan, S. J.: Sedimentation and remineralization associated with biodeposition by the American oyster *Crassostrea virginica* (Gmelin). University of Maryland, College Park, 1987.

Kellogg, M. L., Brush, M., and Cornwell, J. C.: An updated model for estimating the TMDL- related benefits of oyster reef restoration, A final report to The Nature Conservancy and Oyster Recovery Partnership, 2018.

Kelly, C. J., Laramore, S. E., Scarpa, J., and Newell, R. I. E.: Seasonal Comparison of Physiological Adaptation and Growth of Suminoe (Crassostrea ariakensis) and Eastern (Crassostrea virginica) Oysters, J. Shellfish Res., 30, 737–749, https://doi.org/10.2983/035.030.0314, 2011.

Kemp, W., Boynton, W., Adolf, J., Boesch, D., Boicourt, W., Brush, G., Cornwell, J., Fisher, T., Glibert, P., Hagy, J., Harding, L., Houde, E., Kimmel, D., Miller, W., Newell, R., Roman, M., Smith, E., and Stevenson, J.: Eutrophication of Chesapeake Bay: historical trends and ecological interactions, Mar. Ecol. Prog. Ser., 303, 1–29, https://doi.org/10.3354/meps303001, 2005.

Kingsley-Smith, P. R., Harwell, H. D., Kellogg, M. L., Allen, S. M., Allen, S. K., Meritt, D. W., Paynter, K. T., and Luckenbach, M. W.: Survival and Growth of Triploid Crassostrea virginica (Gmelin, 1791) and C. ariakensis (Fujita, 1913) in Bottom Environments of Chesapeake Bay: Implications for an Introduction, J. Shellfish Res., 28, 169–184, https://doi.org/10.2983/035.028.0201, 2009.

La Peyre, M.K., Eberline, B.S., Soniat, T.M. and La Peyre, J.F.: Differences in extreme low salinity timing and duration differentially affect eastern oyster (Crassostrea virginica) size class growth and mortality in Breton Sound, LA, Estuar. Coast. Shelf Sci., 135, 146-157, 2013.

Lake, S. and Brush, M.: Modeling estuarine response to load reductions in a warmer climate: York River Estuary, Virginia, USA, Mar. Ecol. Prog. Ser., 538, 81–98, https://doi.org/10.3354/meps11448, 2015.

Lavaud, R., Peyre, M. K. L., Justic, D., and Peyre, J. F. L.: Dynamic Energy Budget modelling to predict eastern oyster growth, reproduction, and mortality under river management and climate change scenarios, Estuar., Coast. Shelf Sci., 251, 107188, https://doi.org/10.1016/j.ecss.2021.107188, 2021.

Lavaud, R., Peyre, M. K. L., Couvillion, B., Pollack, J. B., Brown, V., Palmer, T. A., and Keim, B.: Predicting restoration and aquaculture potential of eastern oysters through an eco-physiological mechanistic model, Ecol. Model., 489, 110603, https://doi.org/10.1016/j.ecolmodel.2023.110603, 2024.

Lemasson, A. J., Hall-Spencer, J. M., Fletcher, S., Provstgaard-Morys, S., and Knights, A. M.: Indications of future performance of native and non-native adult oysters under acidification and warming, Mar. Environ. Res., 142, 178–189, https://doi.org/10.1016/j.marenvres.2018.10.003, 2018.

Li, M., Lee, Y. J., Testa, J. M., Li, Y., Ni, W., Kemp, W. M., and Toro, D. M. D.: What drives interannual variability of hypoxia in Chesapeake Bay: Climate forcing versus nutrient loading?, Geophys. Res. Lett., 43, 2127–2134, https://doi.org/10.1002/2015gl067334, 2016.

Liddel, M. K.: A von Bertalanffy based model for the estimation of oyster (Crassostrea virginica) growth on restored oyster reefs in Chesapeake Bay, 2008.

Liu, Z., Zhou, Z., Zhang, Y., Wang, L., Song, X., Wang, W., Zheng, Y., Zong, Y., Lv, Z., and Song, L.: Ocean acidification inhibits initial shell formation of oyster larvae by suppressing the biosynthesis of serotonin and dopamine. Sci. Total Environ., 735, 139469, https://doi.org/10.1016/j.scitotenv.2020.139469, 2020.

Loosanoff, V. L.: Some aspects of behavior of oysters at different temperatures, Biol. Bull., 114, 57–70, https://doi.org/10.2307/1538965, 1958.

López-Urrutia, Á., Martin, E. S., Harris, R. P., and Irigoien, X.: Scaling the metabolic balance of the oceans, Proc. Natl. Acad. Sci., 103, 8739–8744, https://doi.org/10.1073/pnas.0601137103, 2006.

Lowe, A. T., Kobelt, J., Horwith, M., and Ruesink, J.: Ability of Eelgrass to Alter Oyster Growth and Physiology Is Spatially Limited and Offset by Increasing Predation Risk, Estuaries Coasts, 42, 743–754, https://doi.org/10.1007/s12237-018-00488-9, 2019.

Lutier, M., Di Poi, C., Gazeau, F., Appolis, A., Le Luyer, J., and Pernet, F.: Revisiting tolerance to ocean acidification: insights from a new framework combining physiological and molecular tipping points of Pacific oyster. Glob. Change Bio., *28*(10), 3333-3348, https://doi.org/10.1111/gcb.16101, 2022.

Mazarrasa, I., Marbà, N., Lovelock, C. E., Serrano, O., Lavery, P. S., Fourqurean, J. W., Kennedy, H., Mateo, M. A., Krause-Jensen, D., Steven, A. D. L., and Duarte, C. M.: Seagrass meadows as a globally significant carbonate reservoir, Biogeosciences, 12, 4993–5003, https://doi.org/10.5194/bg-12-4993-2015, 2015.

Matoo, O. B., Lannig, G., Bock, C., and Sokolova, I. M.: Temperature but not ocean acidification affects energy metabolism and enzyme activities in the blue mussel, Mytilus edulis. Ecol. Evol., 11(7), 3366-3379, https://doi.org/10.1002/ece3.7289, 2021.

Medeiros, I. P. M., and Souza, M. M.: Acid times in physiology: a systematic review of the effects of ocean acidification on calcifying invertebrates. *Environmental Research*, 116019, https://doi.org/10.1016/j.envres.2023.116019, 2023

Melzner, F., Mark, F.C., Seibel, B.A. and Tomanek, L.: Ocean acidification and coastal marine invertebrates: tracking CO_2 effects from seawater to the cell. Annu. Rev. Mar. Sci., 12, pp.499-523, https://doi.org/10.1146/annurev-marine-010419-010658, 2020.

Mitchell, M., Herman, J., Bilkovic, D. M., and Hershner, C.: Marsh persistence under sea-level rise is controlled by multiple, geologically variable stressors, Ecosyst. Heal. Sustain., 3, 1379888, https://doi.org/10.1080/20964129.2017.1396009, 2017.

Mizuta, D. D., Silveira, N., Fischer, C. E., and Lemos, D.: Interannual variation in commercial oyster (Crassostrea gigas) farming in the sea (Florianópolis, Brazil, 27°44′ S; 48°33′ W) in relation to temperature, chlorophyll a and associated oceanographic conditions, Aquaculture, 366, 105–114, https://doi.org/10.1016/j.aquaculture.2012.09.011, 2012.

944 Mizuta, D. D. and Wikfors, G. H.: Seeking the perfect oyster shell: a brief review of current knowledge, Rev. Aquac., 11, 586–
945 602, https://doi.org/10.1111/raq.12247, 2019.

946 Moore, K. A., Orth, R. J., and Wilcox, D. J.: Assessment of the Abundance of Submersed Aquatic Vegetation (SAV)
947 Communities in the Chesapeake Bay and its Use in SAV Management, in: Remote Sensing and Geospatial Technologies for
948 Coastal Ecosystem Assessment and Management, https://doi.org/10.1007/978-3-540-88183-4, 2009.

949 Moore-Maley, B. L., Allen, S. E., and Ianson, D.: Locally driven interannual variability of near-surface pH and ΩA in the
950 Strait of Georgia, J. Geophys. Res.: Oceans, 121, 1600–1625, https://doi.org/10.1002/2015jc011118, 2016.

951 Moriarty, J. M., Friedrichs, M. A. M., and Harris, C. K.: Seabed Resuspension in the Chesapeake Bay: Implications for
952 Biogeochemical Cycling and Hypoxia, Estuaries Coasts, 44, 103–122, https://doi.org/10.1007/s12237-020-00763-8, 2021.

953 Najjar, R. G., Herrmann, M., Valle, S. M. C. D., Friedman, J. R., Friedrichs, M. A. M., Harris, L. A., Shadwick, E. H., Stets,
954 E. G., and Woodland, R. J.: Alkalinity in Tidal Tributaries of the Chesapeake Bay, J. Geophys. Res.: Oceans, 125,
955 https://doi.org/10.1029/2019jc015597, 2020.

956 Newell, R. I. E. and Koch, E. W.: Modeling seagrass density and distribution in response to changes in turbidity stemming
957 from bivalve filtration and seagrass sediment stabilization, Estuaries, 27, 793–806, https://doi.org/10.1007/bf02912041, 2004.

958 Ni, W., Li, M., and Testa, J. M.: Discerning effects of warming, sea level rise and nutrient management on long-term hypoxia
959 trends in Chesapeake Bay, Sci. Total Environ., 737, 139717, https://doi.org/10.1016/j.scitotenv.2020.139717, 2020.

960 Olson, M.: Guide to Using Chesapeake Bay Program Water Quality Monitoring Data, Chesapeake Bay Program, Annapolis,
961 MD, 2012.

962 Nichols, M.M., Kim, S.C. and Brouwer, C.M.: Sediment Characterization of Chesaapeake Bay and Its Tributaries, 1991.

963 Orr, J.C., Fabry, V.J., Aumont, O., Bopp, L., Doney, S.C., Feely, R.A., Gnanadesikan, A., Gruber, N., Ishida, A., Joos, F. and
964 Key, R.M.: Anthropogenic ocean acidification over the twenty-first century and its impact on calcifying organisms,
965 Nature, *437*, 681-686, https://doi.org/10.1038/nature04095, 2005.

966 Orth, R. J., Nowak, J. F., Wilcox, D. J., Whiting, J. R., and Nagey, L. S.: Distribution of Submerged Aquatic Vegetation in the
967 Chesapeake Bay and Tributaries and the Coastal Bays, Am. Zoöl., 3, 315–317, https://doi.org/10.1093/icb/3.3.315, 1998.

968 Pacella, S.R., Brown, C.A., Kaldy, J.E., Labiosa, R.G., Hales, B., Mochon Collura, T.C. and Waldbusser, G.G.: Quantifying
969 the combined impacts of anthropogenic CO2 emissions and watershed alteration on estuary acidification at biologically-
970 relevant time scales: a case study from Tillamook Bay, OR, USA. Front. Mar. Sci., 11, 1293955,
971 https://doi.org/10.3389/fmars.2024.1293955, 2024.

972 Palmer, S. C. J., Gernez, P. M., Thomas, Y., Simis, S., Miller, P. I., Glize, P., and Barillé, L.: Remote Sensing-Driven Pacific
973 Oyster (Crassostrea gigas) Growth Modeling to Inform Offshore Aquaculture Site Selection, Front. Mar. Sci., 6, 802,
974 https://doi.org/10.3389/fmars.2019.00802, 2020.

975 Palmer, S. C. J., Barillé, L., Kay, S., Ciavatta, S., Buck, B., and Gernez, P.: Pacific oyster (Crassostrea gigas) growth modelling
976 and indicators for offshore aquaculture in Europe under climate change uncertainty, Aquaculture, 532, 736116,
977 https://doi.org/10.1016/j.aquaculture.2020.736116, 2021.

Paynter, K. T., Goodwin, J. D., Chen, M. E., Ward, N. J., Sherman, M. W., Meritt, D. W., and Allen, S. K.: *Crassostrea ariakensis* in Chesapeake Bay: Growth, Disease and Mortality in Shallow Subtidal Environments, J. Shellfish Res., 27, 509–515, https://doi.org/10.2983/0730-8000(2008)27[509:caicbg]2.0.co;2, 2008.

Peyre, M. K. L., Eberline, B. S., Soniat, T. M., and Peyre, J. F. L.: Differences in extreme low salinity timing and duration differentially affect eastern oyster (Crassostrea virginica) size class growth and mortality in Breton Sound, LA, Estuar., Coast. Shelf Sci., 135, 146–157, https://doi.org/10.1016/j.ecss.2013.10.001, 2013.

Planton, S., Déqué, M., Chauvin, F., and Terray, L.: Expected impacts of climate change on extreme climate events, C. R. Geosci., 340, 564–574, https://doi.org/10.1016/j.crte.2008.07.009, 2008.

Poach, M., Munroe, D., Vasslides, J., Abrahamsen, I. and Coffey, N.: Monitoring coastal acidification along the US East coast: concerns for shellfish production. Bull. Jap. Fish. Res. Edu. Agen. No, 49, 53-64, 2019.

Ramajo, L., Pérez-León, E., Hendriks, I. E., Marbà, N., Krause-Jensen, D., Sejr, M. K., Blicher, M. E., Lagos, N. A., Olsen, Y. S., and Duarte, C. M.: Food supply confers calcifiers resistance to ocean acidification, Sci. Rep., 6, 19374, https://doi.org/10.1038/srep19374, 2016.

Raymond, P. A., Bauer, J. E., and Cole, J. J.: Atmospheric CO_2 evasion, dissolved inorganic carbon production, and net heterotrophy in the York River estuary, Limnol. Oceanogr., 45, 1707–1717, https://doi.org/10.4319/lo.2000.45.8.1707, 2000.

Riahi, K., Rao, S., Krey, V., Cho, C., Chirkov, V., Fischer, G., Kindermann, G., Nakicenovic, N., and Rafaj, P.: RCP 8.5—A scenario of comparatively high greenhouse gas emissions, Clim. Chang., 109, 33, https://doi.org/10.1007/s10584-011-0149-y, 2011.

Redfield, A.C.: On the proportions of organic derivatives in sea water and their relation to the composition of plankton, University Press of Liverpool, Liverpool, UK, 1934.

Reid, J.M., Reid, J.A., Jenkins, C.J., Hastings, M.E., Williams, S.J. and Poppe, L.J.: usSEABED: Atlantic coast offshore surficial sediment data release, US Geological Survey Data Series, 118, 2005.

Rivest, E.B., Brush, M., Zimmerman, R., Hill., V," Can Meadows of Submerged Aquatic Vegetation (SAV) Mitigate Ocean Acidification Thresholds for Eastern Oysters in the Chesapeake Bay? Final report, NOAA Ocean Acidification Program. Award number NA18NOS4780177, 2023.

Roden, E. and Tuttle, J.: Inorganic sulfur cycling in mid and lower Chesapeake Bay sediments, Mar. Ecol. Prog. Ser., 93, 101–118, https://doi.org/10.3354/meps093101, 1993.

Rybovich, M., Peyre, M. K. L., Hall, S. G., and Peyre, J. F. L.: Increased Temperatures Combined with Lowered Salinities Differentially Impact Oyster Size Class Growth and Mortality, J. Shellfish Res., 35, 101–113, https://doi.org/10.2983/035.035.0112, 2016.

Saavedra, L., Bastías, M., Mendoza, P., Lagos, N. A., García-Herrera, C., Ponce, V., Alvarez, F., and Llanos-Rivera, A.: Environmental correlates of oyster farming in an upwelling system: Implication upon growth, biomass production, shell strength and organic composition, Mar. Environ. Res., https://doi.org/10.1016/j.marenvres.2024.106489, 2024.

Salisbury, J., Green, M., Hunt, C., and Campbell, J.: Coastal Acidification by Rivers: A Threat to Shellfish?, Eos, Trans. Am. Geophys. Union, 89, 513–513, https://doi.org/10.1029/2008eo500001, 2008.

Schwaner, C., Barbosa, M., Schwemmer, T. G., Espinosa, E. P., and Allam, B.: Increased Food Resources Help Eastern Oyster Mitigate the Negative Impacts of Coastal Acidification, Animals, 13, 1161, https://doi.org/10.3390/ani13071161, 2023.

Simone, M. N., Schulz, K. G., Oakes, J. M., and Eyre, B. D.: Warming and ocean acidification may decrease estuarine dissolved organic carbon export to the ocean, Biogeosciences, 18, 1823–1838, https://doi.org/10.5194/bg-18-1823-2021, 2021.

Nixon, S.W.: Coastal marine eutrophication: A definition, social causes, and future concerns, Ophelia, 41, 199-219, htpps://doi.org/10.1080/00785236.1995.10422044, 1995.

Shadwick, E. H., Friedrichs, M. A. M., Najjar, R. G., Meo, O. A. D., Friedman, J. R., Da, F., and Reay, W. G.: High-Frequency CO_2 System Variability Over the Winter-to-Spring Transition in a Coastal Plain Estuary, J. Geophys. Res.: Oceans, 124, 7626–7642, https://doi.org/10.1029/2019jc015246, 2019.

Shchepetkin, A. F. and McWilliams, J. C.: The regional oceanic modeling system (ROMS): a split-explicit, free-surface, topography-following-coordinate oceanic model, Ocean Model., 9, 347–404, https://doi.org/10.1016/j.ocemod.2004.08.002, 2005.

Shen, C., Testa, J. M., Li, M., Cai, W., Waldbusser, G. G., Ni, W., Kemp, W. M., Cornwell, J., Chen, B., Brodeur, J., and Su, J.: Controls on Carbonate System Dynamics in a Coastal Plain Estuary: A Modeling Study, J. Geophys. Res.: Biogeosciences, 124, 61–78, https://doi.org/10.1029/2018jg004802, 2019a.

Shen, C., Testa, J. M., Ni, W., Cai, W., Li, M., and Kemp, W. M.: Ecosystem Metabolism and Carbon Balance in Chesapeake Bay: A 30-Year Analysis Using a Coupled Hydrodynamic-Biogeochemical Model, J. Geophys. Res.: Oceans, 124, 6141–6153, https://doi.org/10.1029/2019jc015296, 2019b.

Shen, C., Testa, J. M., Li, M., and Cai, W.: Understanding Anthropogenic Impacts on pH and Aragonite Saturation State in Chesapeake Bay: Insights From a 30-Year Model Study, J. Geophys. Res.: Biogeosciences, 125, https://doi.org/10.1029/2019jg005620, 2020.

Siedlecki, S. A., Pilcher, D., Howard, E. M., Deutsch, C., MacCready, P., Norton, E. L., Frenzel, H., Newton, J., Feely, R. A., Alin, S. R., and Klinger, T.: Coastal processes modify projections of some climate-driven stressors in the California Current System, Biogeosciences, 18, 2871–2890, https://doi.org/10.5194/bg-18-2871-2021, 2021a.

Siedlecki, S., Salisbury, J., Gledhill, D., Bastidas, C., Meseck, S., McGarry, K., Hunt, C., Alexander, M., Lavoie, D., Wang, Z., Scott, J., Brady, D., Mlsna, I., Azetsu-Scott, K., Liberti, C., Melrose, D., White, M., Pershing, A., Vandemark, D., Townsend, D., Chen, C., Mook, W., and Morrison, R.: Projecting ocean acidification impacts for the Gulf of Maine to 2050, Elem.: Sci. Anthr., 9, https://doi.org/10.1525/elementa.2020.00062, 2021b.

Speights, C. J., Silliman, B. R., and McCoy, M. W.: The effects of elevated temperature and dissolved ρCO_2 on a marine foundation species, Ecol. Evol., 7, 3808–3814, https://doi.org/10.1002/ece3.2969, 2017.

1043 Simpson, E., Ianson, D., Kohfeld, K. E., Franco, A. C., Covert, P. A., Davelaar, M., and Perreault, Y.: Variability and drivers
1044 of carbonate chemistry at shellfish aquaculture sites in the Salish Sea, British Columbia. Biogeosciences, 21, 1323-1353,
1045 https://doi.org/10.5194/bg-21-1323-2024, 2024.

1046 Stevens, A. and Gobler, C.: Interactive effects of acidification, hypoxia, and thermal stress on growth, respiration, and survival
1047 of four North Atlantic bivalves, Mar. Ecol. Prog. Ser., 604, 143–161, https://doi.org/10.3354/meps12725, 2018.

1048 St-Laurent, P. and Friedrichs, M. A. M.: On the Sensitivity of Coastal Hypoxia to Its External Physical Forcings, J. Adv.
1049 Model. Earth Syst., 16, https://doi.org/10.1029/2023ms003845, 2024.

1050 St-Laurent, P., Friedrichs, M. A. M., Najjar, R. G., Shadwick, E. H., Tian, H., and Yao, Y.: Relative impacts of global changes
1051 and regional watershed changes on the inorganic carbon balance of the Chesapeake Bay, Biogeosciences, 17, 3779–3796,
1052 https://doi.org/10.5194/bg-17-3779-2020, 2020.

1053 Su, J., Cai, W.-J., Brodeur, J., Chen, B., Hussain, N., Yao, Y., Ni, C., Testa, J. M., Li, M., Xie, X., Ni, W., Scaboo, K. M., Xu,
1054 Y., Cornwell, J., Gurbisz, C., Owens, M. S., Waldbusser, G. G., Dai, M., and Kemp, W. M.: Chesapeake Bay acidification
1055 buffered by spatially decoupled carbonate mineral cycling, Nat. Geosci., 13, 441–447, https://doi.org/10.1038/s41561-020-
1056 0584-3, 2020.

1057 Swam, L. M., Couvillion, B., Callam, B., Peyre, J. F. L., and Peyre, M. K. L.: Defining oyster resource zones across coastal
1058 Louisiana for restoration and aquaculture, Ocean Coast. Manag., 225, 106178,
1059 https://doi.org/10.1016/j.ocecoaman.2022.106178, 2022.

1060 Talmage, S. C. and Gobler, C. J.: Effects of Elevated Temperature and Carbon Dioxide on the Growth and Survival of Larvae
1061 and Juveniles of Three Species of Northwest Atlantic Bivalves, PLoS ONE, 6, e26941,
1062 https://doi.org/10.1371/journal.pone.0026941, 2011.

1063 Tian, R., Cerco, C. F., Bhatt, G., Linker, L. C., and Shenk, G. W.: Mechanisms Controlling Climate Warming Impact on the
1064 Occurrence of Hypoxia in Chesapeake Bay, JAWRA J. Am. Water Resour. Assoc., 58, 855–875, https://doi.org/10.1111/1752-
1065 1688.12907, 2022.

1066 Thomsen, J., Haynert, K., Wegner, K. M., and Melzner, F.: Impact of seawater carbonate chemistry on the calcification of
1067 marine bivalves, Biogeosciences, 12, 4209–4220, https://doi.org/10.5194/bg-12-4209-2015, 2015.

1068 Turner, J. S., St-Laurent, P., Friedrichs, M. A. M., and Friedrichs, C. T.: Effects of reduced shoreline erosion on Chesapeake
1069 Bay water clarity, Sci. Total Environ., 769, 145157, https://doi.org/10.1016/j.scitotenv.2021.145157, 2021.

1070 USDA National Agricultural Statistics Service, 2023 Census of Aquaculture, 2023.

1071 van Heuven, S., D. Pierrot, J.W.B. Lewis, R.E., and Wallace, D.W.R.: MATLAB Program Developed for CO_2 System
1072 Calculations. ORNL/CDIAC-105b. Carbon Dioxide Information Analysis Center, Oak Ridge National Laboratory, U.S.
1073 Department of Energy, Oak Ridge, Tennessee. https://doi.org/10.3334/CDIAC/otg.CO2SYS_MATLAB_v1.1, 2011.

1074 VOSARA: https://cmap22.vims.edu/VOSARA/,last access: 28 January 2024.

1075 Waldbusser, G. G., Voigt, E. P., Bergschneider, H., Green, M. A., and Newell, R. I. E.: Biocalcification in the Eastern Oyster
1076 (Crassostrea virginica) in Relation to Long-term Trends in Chesapeake Bay pH, Estuaries Coasts, 34, 221–231,
1077 https://doi.org/10.1007/s12237-010-9307-0, 2011.

1078 Wallace, R. B., Baumann, H., Grear, J. S., Aller, R. C., and Gobler, C. J.: Coastal ocean acidification: The other eutrophication
1079 problem, Estuar., Coast. Shelf Sci., 148, 1–13, https://doi.org/10.1016/j.ecss.2014.05.027, 2014.

1080 Warner, J. C., Defne, Z., Haas, K., and Arango, H. G.: A wetting and drying scheme for ROMS, Comput. Geosci., 58, 54–61,
1081 https://doi.org/10.1016/j.cageo.2013.05.004, 2013.

1082 Zhang, Q., Fisher, T. R., Trentacoste, E. M., Buchanan, C., Gustafson, A. B., Karrh, R., Murphy, R. R., Keisman, J., Wu, C.,
1083 Tian, R., Testa, J. M., and Tango, P. J.: Nutrient limitation of phytoplankton in Chesapeake Bay: Development of an empirical
1084 approach for water-quality management, Water Res., 188, 116407, https://doi.org/10.1016/j.watres.2020.116407, 2021.

1085

1086 Table 1. Experimental design for future simulations conducted for comparison to reference run. Model forcings include a

1087 combination of 2017 (reference) and 2067 (future) inputs of atmospheric CO_2, atmospheric temperature, and terrestrial nutrient

1088 loadings.

Future Simulation Name	Atmospheric CO_2	Atmospheric Temperature	Terrestrial inputs
Combined Future	Future	Future	TMDL[a]
AtmCO$_2$	Future	Reference	Reference
Temp	Reference	Future	Reference
TMDL	Reference	Reference	TMDL
AtmCO$_2$ + Temp	Future	Future	Reference

1089 [a]TMDL (Total Maximum Daily Load) forcing includes inputs of nitrate, ammonium, and dissolved and particulate organic

1090 matter under the assumption that the nutrient reduction goals (EPA, 2010) are met.

1091   Table 2. Model skill statistics (mean ± standard deviation) comparing bottom grid cells from the reference run to Chesapeake

1092   Bay Program observations from the same station location and time, within the bottom 10% of the water column.

Variable	Model	Observation	Model Bias	RMSD[a]
Temperature (°C) n = 130	17.0 ± 9	16.7 ± 9	+ 0.2	0.7
Salinity n = 127	13.9 ± 7	15.4 ± 7	-1.5	2.7
Oxygen (mg O_2 L^{-1}) n = 130	8.0 ± 2.3	7.2 ± 2.9	+0.9	1.3
pH n = 74	7.8 ± 0.4	7.6 ± 0.4	+ 0.2	0.4
TSS (mg L^{-1}) n = 74	44 ± 34	45 ± 54	-1.1	48.3
POC (g C m^{-3}) n = 74	0.7 ± 0.3	1.7 ± 2.1	-1.0	2.4

1093   [a]RMSD = root mean squared difference

1094 Table 3. Bottom environmental variables for each model simulation (annual mean ± standard deviation) for grid cells that
1095 support oyster growth in the reference run (defined as those with greater than 1g dry tissue weight after one year of growth;
1096 Fig. S2). Analogous results averaged over all model grid cells are shown in Table S5.

Model Simulation	Temperature (°C)	Salinity	POC (g C m^{-3})	Ω_{Ca}	Dissolved Oxygen (mg O$_2$ L^{-1})	TSS (mg L^{-1})
Reference	17.0 ± 0.7	15.7 ± 2.1	1.12 ± 0.1	2.5 ± 0.49	9.1 ± 0.6	11.4 ± 5.8
Combined Future	18.5 ± 0.8	16.0 ± 2.1	1.03 ± 0.1	1.6 ± 0.35	8.7 ± 0.6	11.1 ± 5.9
AtmCO$_2$	17.0 ± 0.7	15.7 ± 2.1	1.12 ± 0.1	1.6 ± 0.35	9.1 ± 0.6	11.4 ± 5.8
Temp	18.5 ± 0.8	16.0 ± 2.1	1.07 ± 0.1	2.5 ± 0.41	8.8 ± 0.6	11.1 ± 5.9
TMDL	17.0 ± 0.7	15.7 ± 2.1	1.08 ± 0.1	2.4 ± 0.53	9.1 ± 0.6	11.2 ± 5.9
Temp + CO$_2$	18.5 ± 0.8	16.0 ± 2.1	1.07 ± 0.1	1.7 ± 0.33	8.8 ± 0.6	11.1 ± 5.9

1097

1098   Table 4. Modeled oyster characteristics from the end of each simulation (mean ± standard deviation) over grid cells that support

1099   oyster growth in the reference run (defined as those with greater than 1g dry tissue weight after one year of growth; Fig. S2).

Model Simulation	Shell Weight (g)	Tissue Weight (g)	Shell Thickness (g mm^{-1})
Reference	16.8 ± 10.9	2.2 ± 1.5	0.18 ± 0.08
Combined Future	5.4 ± 5.7	0.9 ± 0.8	0.07 ± 0.05
AtmCO$_2$	10.5 ± 8.0	2.2 ± 1.5	0.12 ± 0.06
Temp	9.7 ± 9.1	1.2 ± 1.1	0.10 ± 0.07
TMDL	13.1 ± 8.2	1.7 ± 1.2	0.15 ± 0.06
Temp + CO$_2$	6.6 ± 7.1	1.2 ± 1.1	0.08 ± 0.06

1100
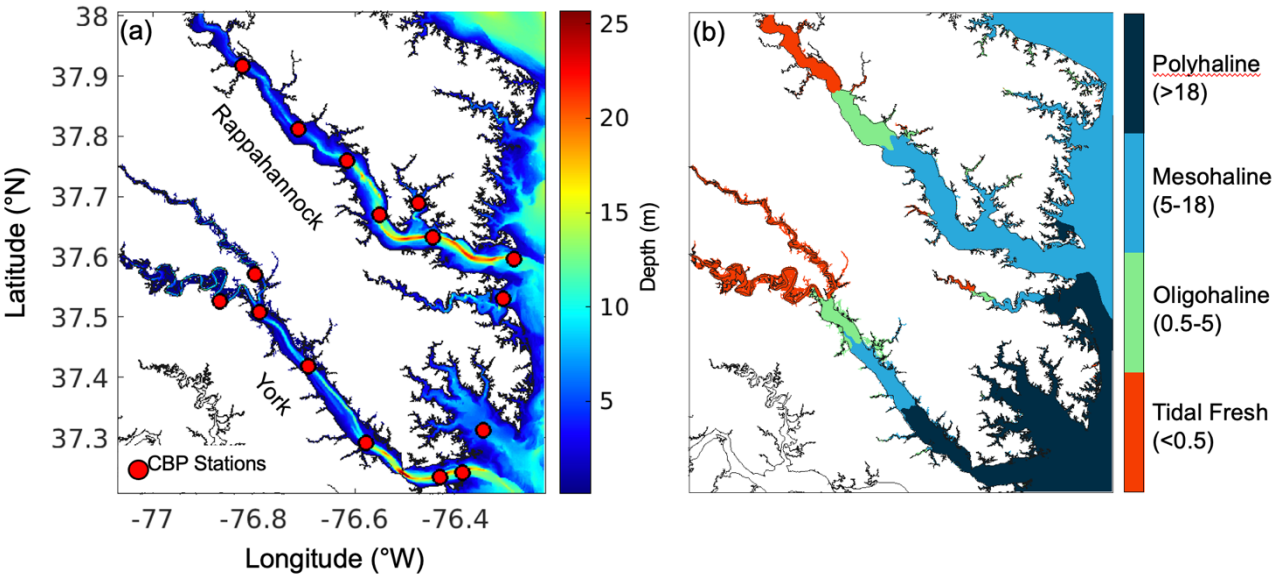
1103 Figure 1. ROMS-ECBO model domain of Chesapeake Bay tributaries illustrating (a) bathymetry in meters and locations of
1104 Chesapeake Bay Program (CBP) water quality monitoring stations (red circles) and (b) bottom salinity zones.
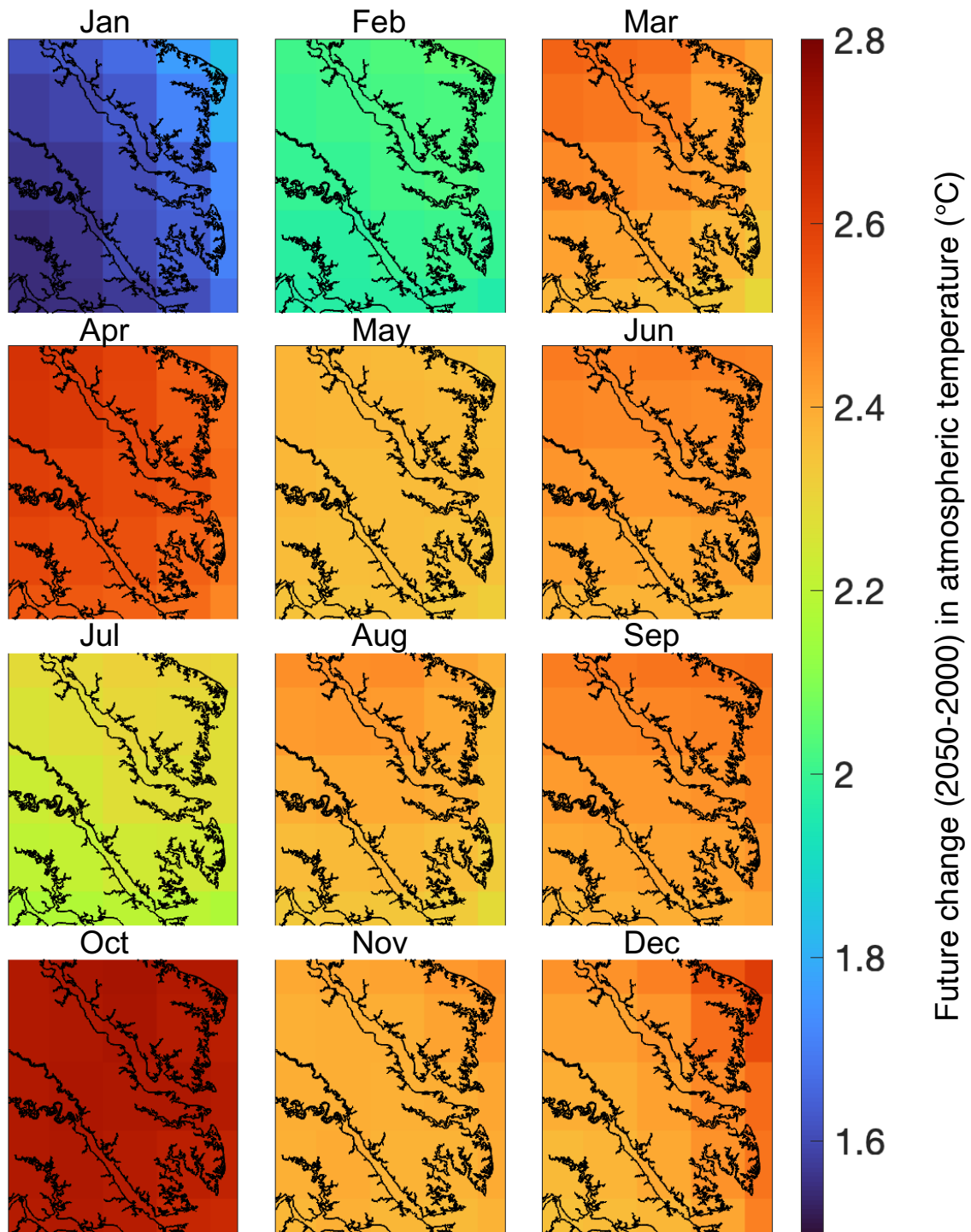
1105   Figure 2. Monthly-averaged 50-year atmospheric temperature differences over the ROMS-ECBO model domain calculated as projections
1106   from 2050 minus those from 2000.
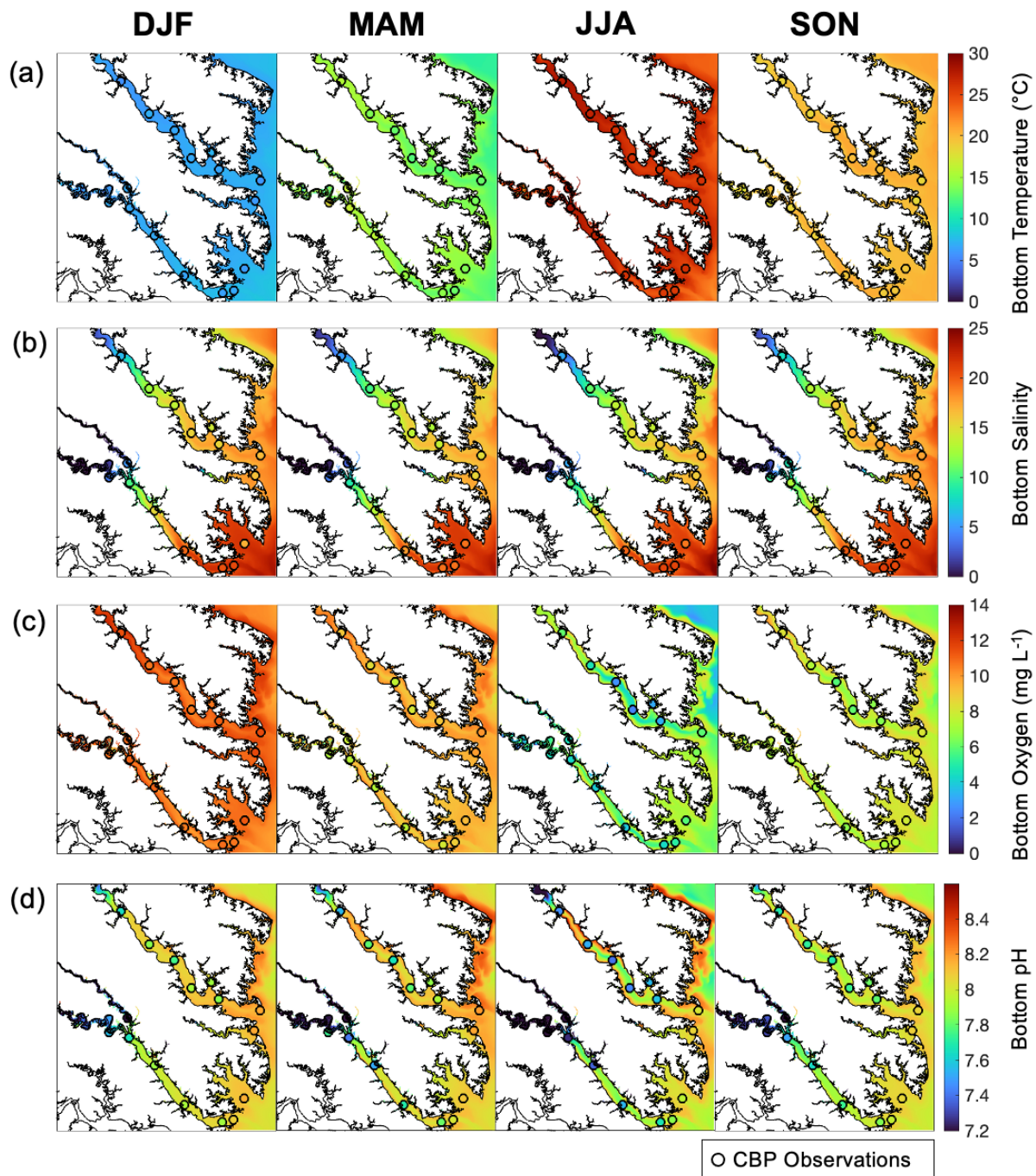
1107   Figure 3. Seasonally-averaged bottom (a) temperature, (b) salinity, (c) dissolved oxygen, and (d) pH from the reference run.
1108   Circles represent seasonal decadal-averaged *in situ* observations at Chesapeake Bay Program stations (2010-2020). (DJF =
1109   winter, MAM = spring, JJA = summer, and SON = fall).
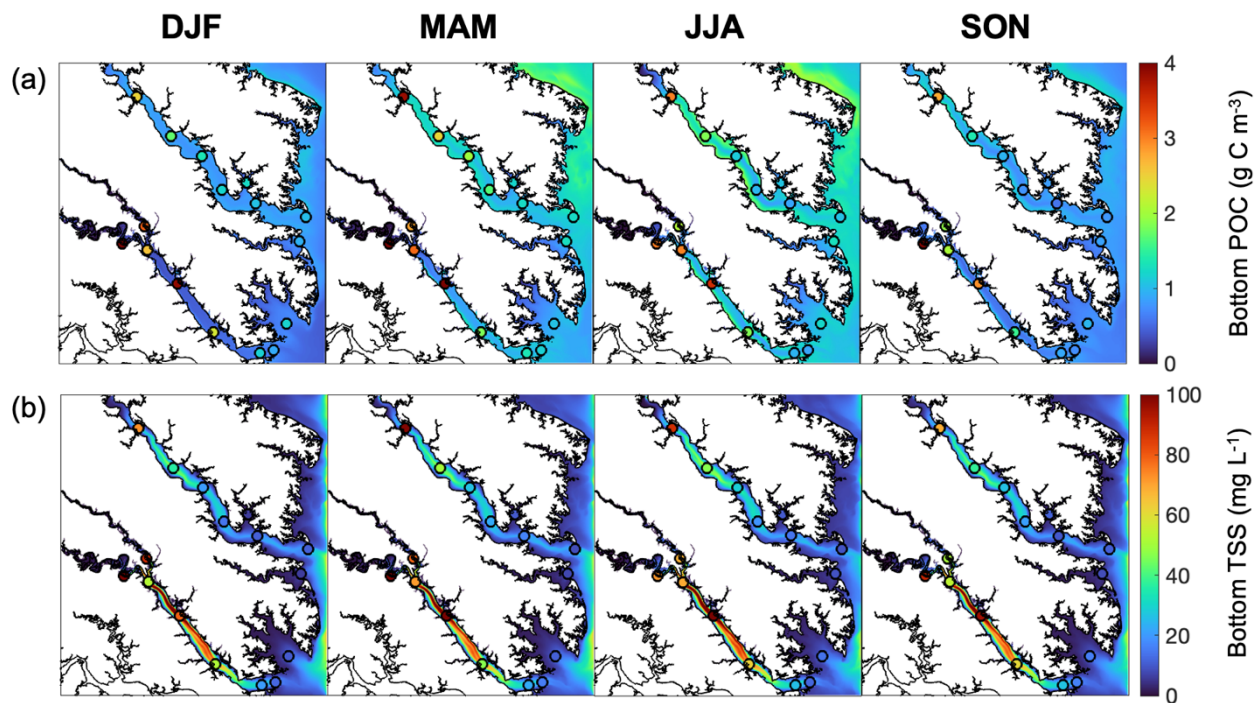
1110   Figure 4. Seasonally-averaged bottom (a) POC and (b) TSS from output of the reference run of the ROMS-ECBO model.

1111   Circles represent seasonal decadal-averaged bottom measurements at Chesapeake Bay Program stations (2010-2020). (DJF =

1112   winter, MAM = spring, JJA = summer, and SON = fall).
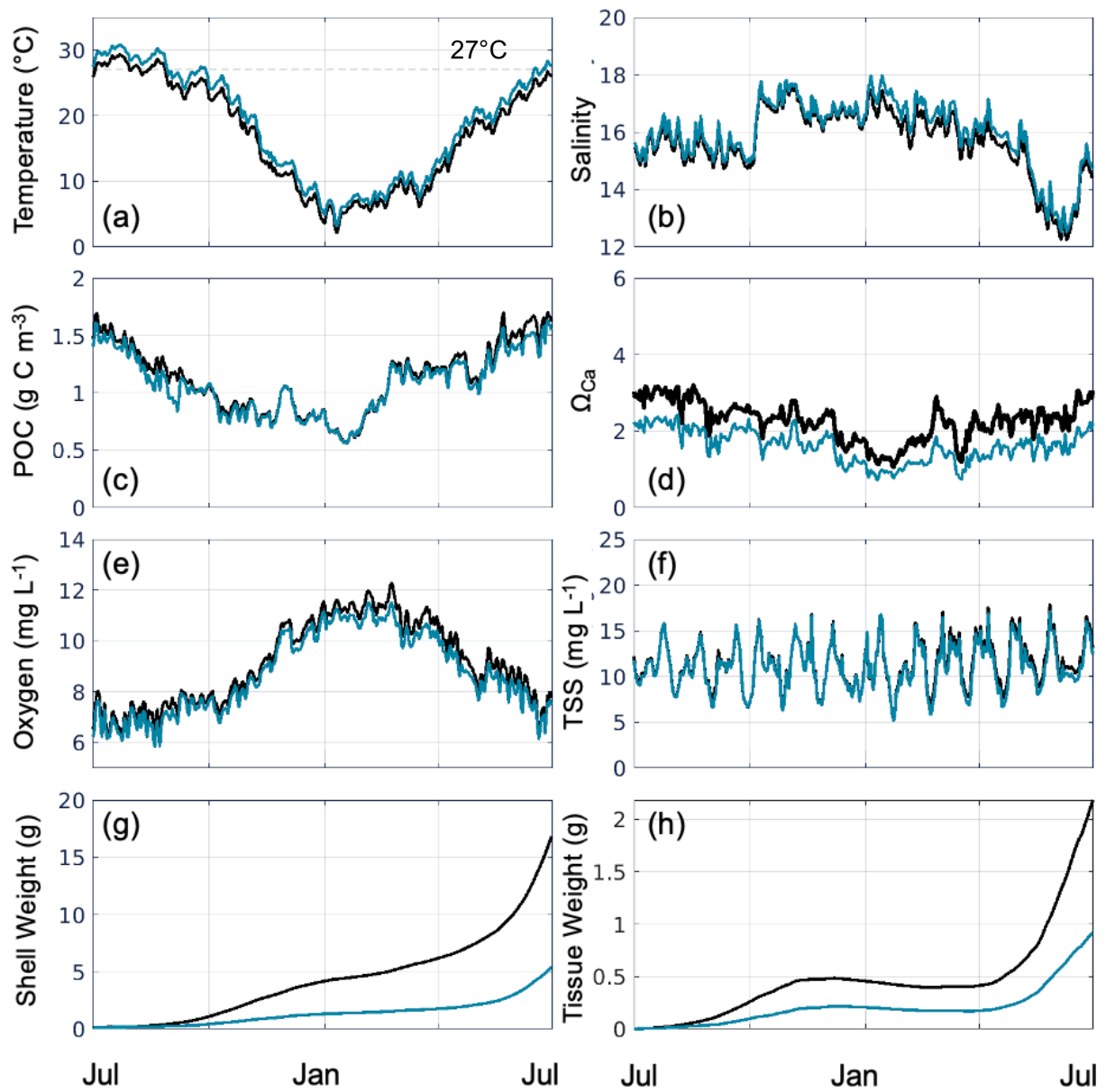
Figure 5. Time series of daily bottom (a) temperature, (b) salinity, c) POC, (d) ΩCa, (e) oxygen, (f) TSS, (g) shell weight, and (h) tissue weight, averaged over grid cells that support oyster growth in the reference run, for the present-day reference run (black line) and Combined Future simulation (blue line). The horizontal dashed line in (a) represents the optimal filtration temperature in EcoOyster (27°C).
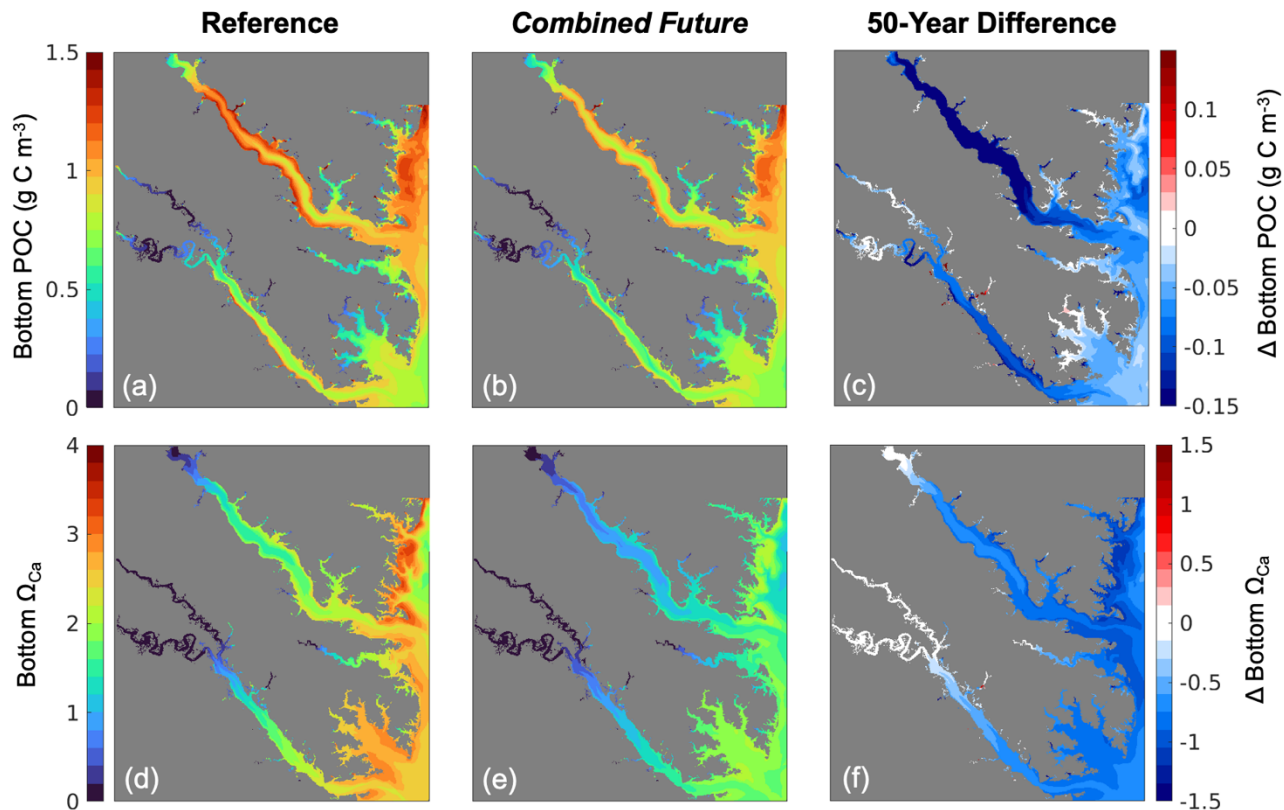
1117

Figure 6. Annual mean bottom (a-c) POC and (d-f) Ω_{Ca} from (a,d) the present-day reference run, (b,e) the *Combined Future* simulation, and (c,f) the difference between (a) and (b), i.e., *Combined Future* minus reference.
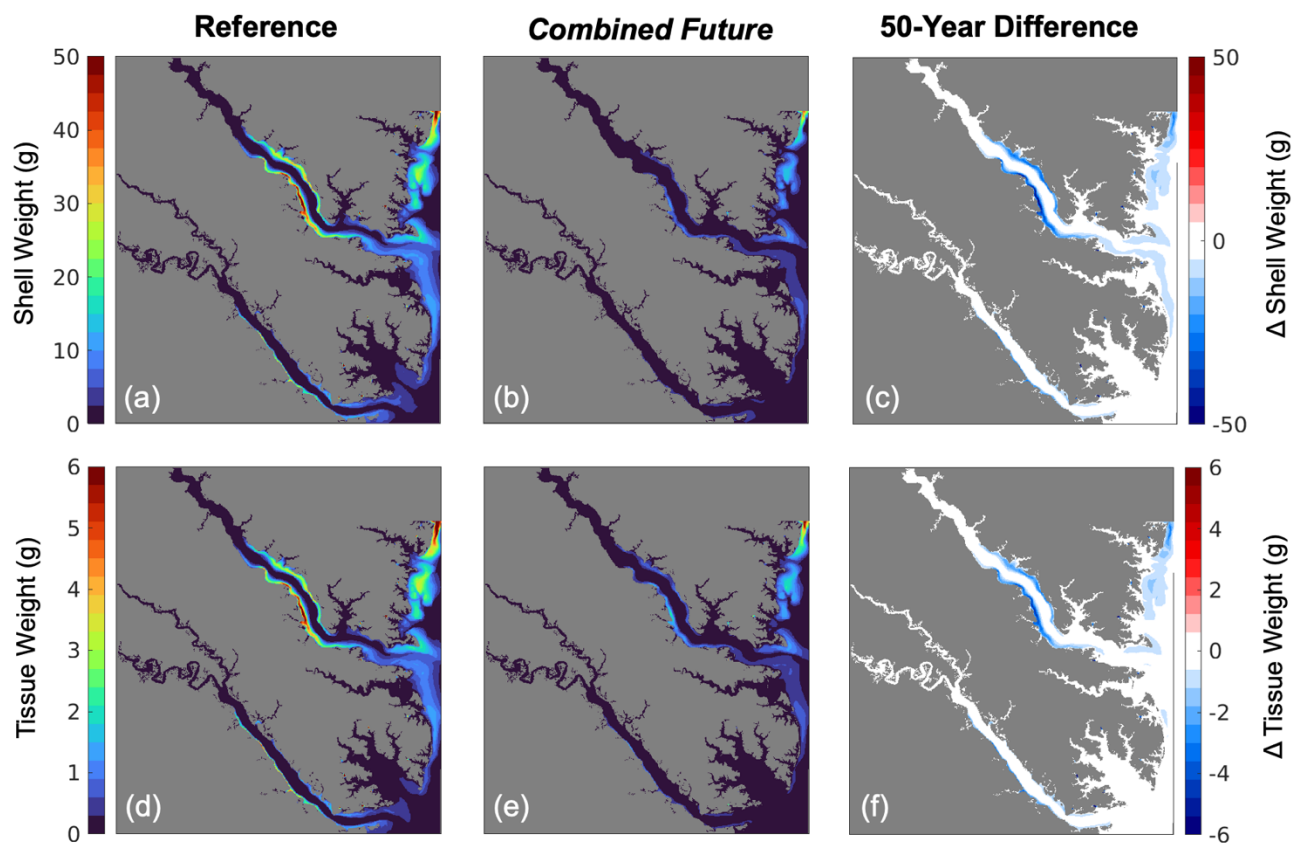
Figure 7. (a-c) Shell weight and (d-f) tissue weight at the end of the one-year simulation from (a,d) the present-day reference run, (b,e) the *Combined Future* run, and (c,f) their difference, i.e., *Combined Future* minus reference.

1122
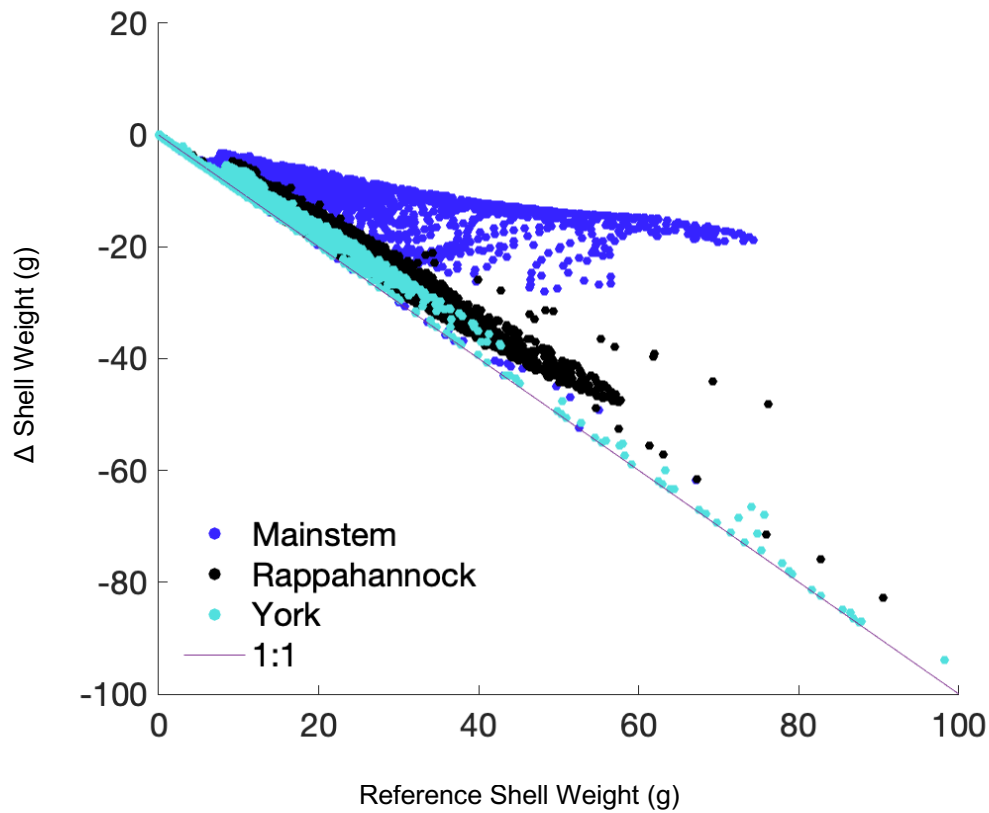
1123   Figure 8. Difference in shell weight at the end of the one-year simulation between the *Combined Future* run and the reference
1124   run, i.e., *Combined Future* minus reference, colored by region. Each point represents a grid cell where oyster growth occurs
1125   in the reference run.
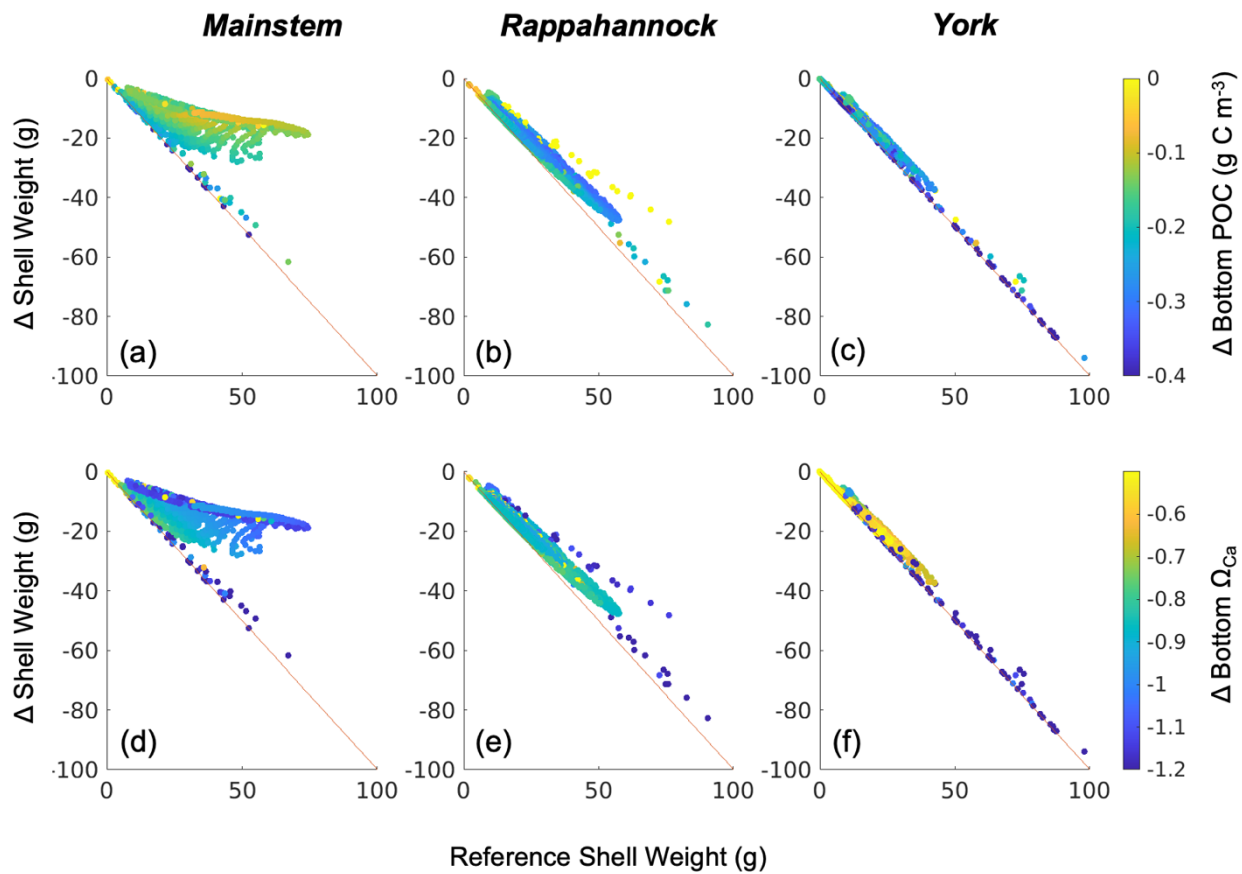
1126
1127 Figure 9. Difference in shell weight at the end of the one-year simulation between the *Combined Future* run and the reference
1128 run colored by (a-c) change in POC and (d-f) change in bottom Ω_{Ca} (i.e. *Combined Future* minus reference) for grid cells that
1129 support oyster growth. Results are presented for (a,d) the mainstem shoal only, (b,e) the Rappahannock River only, and (c,f)
1130 the York River only.
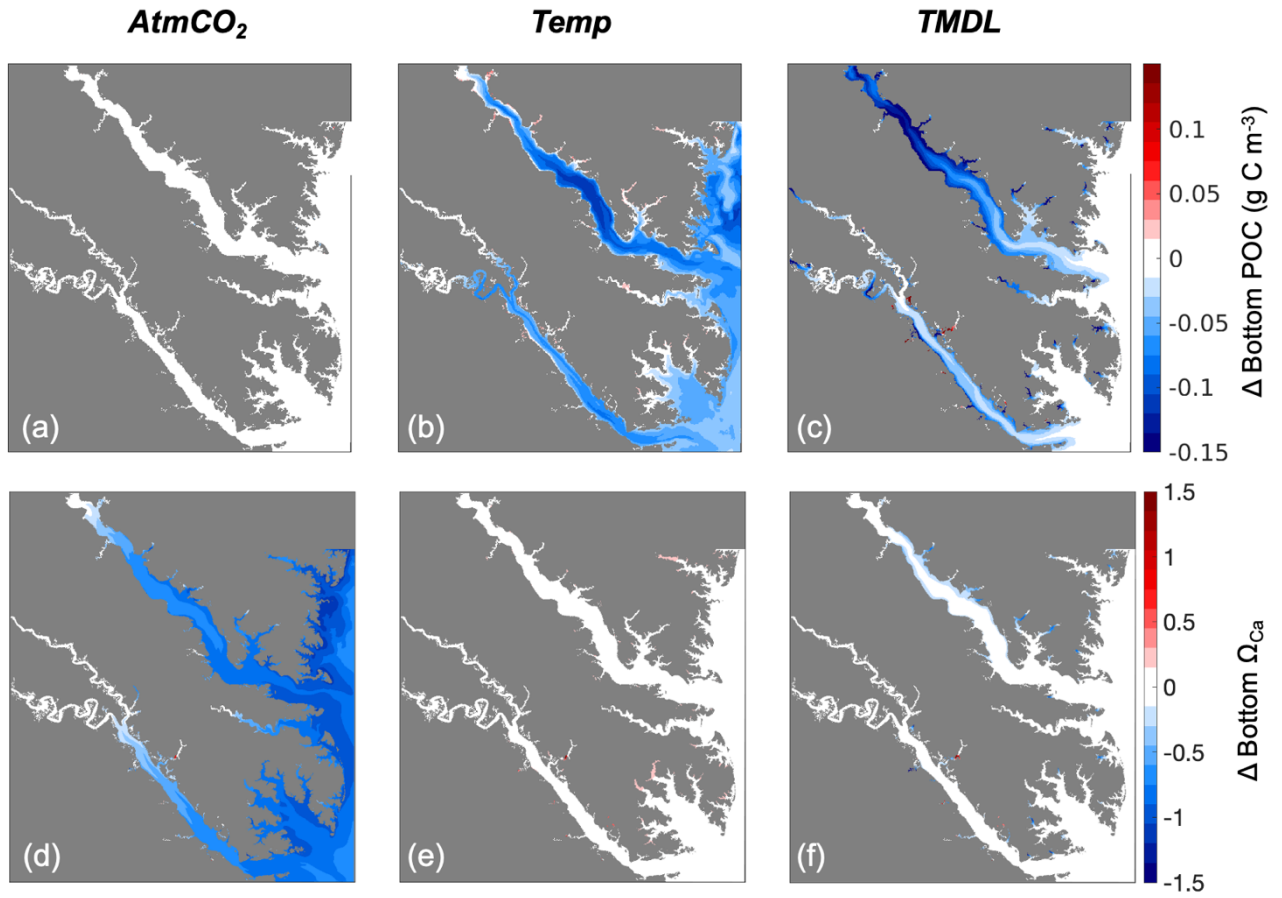
Figure 10. Differences in annual averaged (a-c) bottom POC and (d-f) bottom Ω_{Ca} (d-f) for three sensitivity experiments: (a) AtmCO2, (b) Temp, and (c) TMDL. Differences represent future results minus those from the present-day reference run.
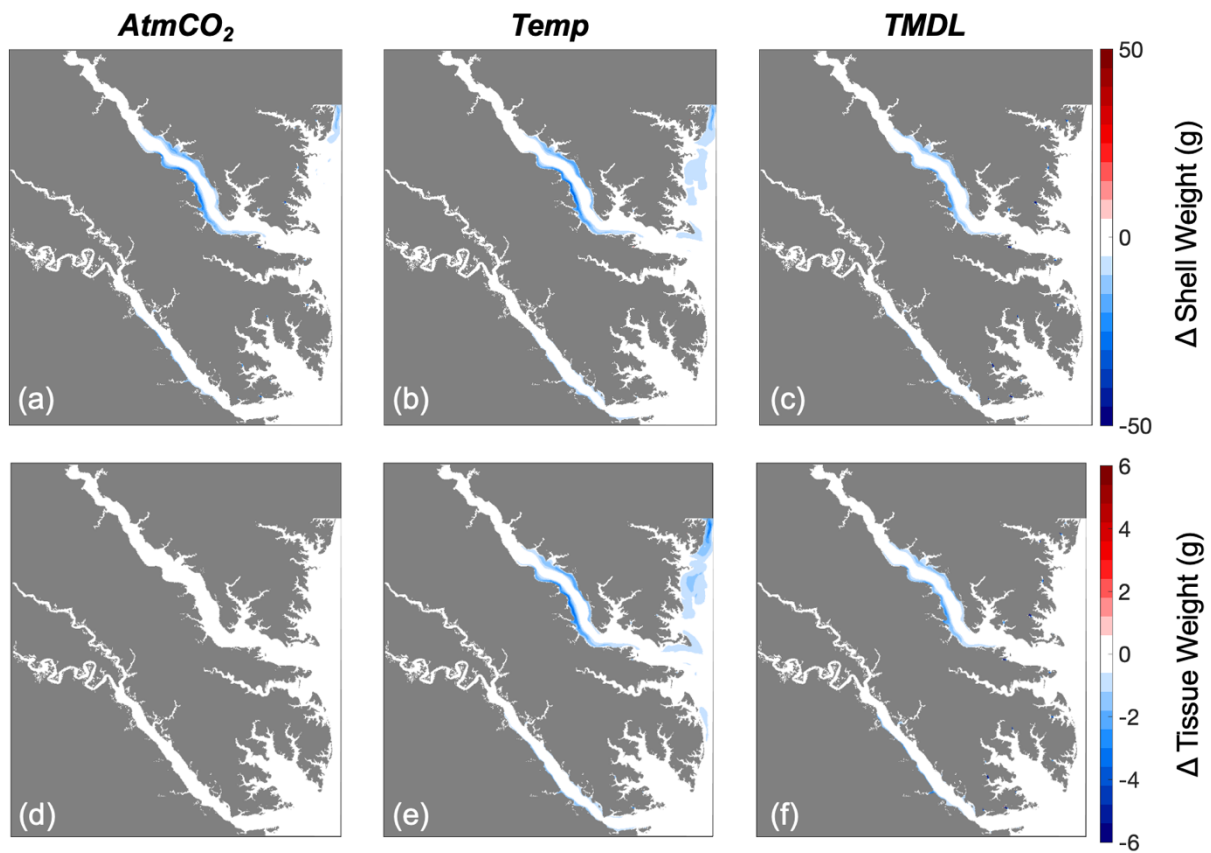
1133   Figure 11. Differences in (a-c) shell weight and (d-f) tissue weight at the end of the one-year simulation for three sensitivity
1134   experiments: (a) AtmCO$_2$, (b) Temp, and (c) TMDL. Differences represent future results minus those from the present-day
1135   reference run.

1136